Geological Society of America Bulletin, published online on 21 November 2012 as doi:10.1130/B30626.1

Geological Society of America Bulletin

U-Pb zircon geochronology of major lithologic units in the eastern Himalaya: Implications for the origin and assembly of Himalayan rocks

A. Alexander G. Webb, An Yin and Chandra S. Dubey

Geological Society of America Bulletin published online 21 November 2012;
doi: 10.1130/B30626.1

Notes

Geological Society of America Bulletin, published online on 21 November 2012 as doi:10.1130/B30626.1

U-Pb zircon geochronology of major lithologic units in the eastern Himalaya: Implications for the origin and assembly of Himalayan rocks

A. Alexander G. Webb[1,†], An Yin[2], and Chandra S. Dubey[3]
[1]*Department of Geology and Geophysics, Louisiana State University, Baton Rouge, Louisiana 70803, USA*
[2]*Department of Earth and Space Sciences and Institute of Geophysics and Planetary Physics, University of California, Los Angeles, California 90095, USA*
[3]*Department of Geology, Delhi University, Delhi-110007, India*

ABSTRACT

Models for the origin and deformation of Himalayan rocks are dependent upon geometric and age relationships between major units. We present field mapping and U-Pb dating of igneous and detrital zircons that establish the lithostratigraphic architecture of the eastern Himalaya, revealing that: (1) the South Tibet detachment along the Bhutan-China border is a top-to-the-north ductile shear zone; (2) Late Triassic and Early Cretaceous sedimentary samples from the northern Indian margin show a similar age range of detrital zircons from ca. 3500 Ma to ca. 200 Ma, but the Late Triassic rocks are distinguished by a significant age cluster between ca. 280 and ca. 220 Ma and a well-defined age peak at ca. 570 Ma, (3) an augen gneiss in the South Tibet detachment shear zone in southeast Tibet has a Cambrian–Ordovician crystallization age, (4) Main Central thrust hanging-wall paragneiss and footwall quartzites from the far western Arunachal Himalaya share similar provenance and Late Proterozoic maximum depositional ages, and (5) Main Central thrust footwall metagraywacke from the central western Arunachal Himalaya has a Paleoproterozoic maximum depositional age, indicated by a single prominent age peak of ca. 1780 Ma. Recent work in the eastern Himalaya demonstrates that in the early-middle Miocene, the Himalayan crystalline core here was emplaced southward between two subhorizontal shear zones that merge to the south. A proposed subsequent (middle Miocene) brittle low-angle normal fault accomplishing exhumation of these rocks along the range crest can be precluded because new and existing mapping demonstrates only a ductile shear zone here. The ca. 280–220 Ma detrital zircons of the Late Triassic strata are derived from an arc developed along the northern margin of the Lhasa terrane. Detritus from this arc was deposited on the northern margin of India during India-Lhasa rifting. Along-strike heterogeneity in Main Central thrust footwall chronostratigraphy is indicated by detrital zircon age spectrum differences from central western to far western Arunachal. Nonetheless, the Late Proterozoic rocks in the Main Central thrust hanging wall and footwall in far western Arunachal can be correlated to each other, and to previously analyzed rocks in the South Tibet detachment hanging wall to the west and in the Indian craton to the south. These findings are synthesized in a reconstruction showing Late Triassic India-Lhasa rifting and Cenozoic eastern Himalayan construction via in situ thrusting of basement and cover sequences along the north Indian margin.

INTRODUCTION

Simple questions of Himalayan geology—i.e., where does Himalayan material originate, and how was it assembled?—may have surprisingly complex answers. The geometric framework of the Himalayan orogen was established by Heim and Gansser (1939), who divided it into a generally north-dipping stack of three units separated from foreland detritus to the south and Asian plate rocks to the north. These units are now termed the Lesser Himalayan Sequence (LHS, at the base), the Greater Himalayan Crystalline complex (GHC, in the middle), and the Tethyan Himalayan Sequence (THS, at the top) (Fig. 1; e.g., Yin, 2006). Early models for the origin and assembly of these units were straightforward, suggesting that as the southern front of the India-Asia collision, the Himalayan orogen was generated via in situ thrusting of Indian basement and cover sequences (Argand, 1924; Heim and Gansser, 1939; Dewey and Bird, 1970; Le Fort, 1975).

Assembling the Himalaya

Structural evidence provided the first intimation that the kinematic evolution might have involved complexities beyond thrust tectonics. Recognition of top-to-the-north shear structures along the gently north-dipping GHC-THS contact at the range crest (e.g., Caby et al., 1983; Burg et al., 1984) quickly led to acceptance of a new paradigm—that this contact was defined by a top-to-the-north low-angle normal fault system with tens or even hundreds of kilometers of slip (e.g., Searle, 1986; Burchfiel et al., 1992). This fault system is termed the South Tibet detachment. Current models for the assembly of the Himalayan units focus on the emplacement of the GHC along the South Tibet detachment and the Main Central thrust, which emplaced the GHC southward over the LHS.

The first kinematic model proposed for this emplacement is *wedge extrusion*, in which the GHC extruded southward between the other two units as a northward-tapering wedge (Fig. 2A; Burchfiel and Royden, 1985). Some recent workers associated these kinematics with critical taper–Coulomb wedge theory (e.g., Robinson et al., 2006; Kohn, 2008; Zhang et al., 2011), which suggests that normal faulting may occur during collapse of overthickened thrust wedges (e.g., Davis et al., 1983; Dahlen, 1990). In the second kinematic model, *channel flow–focused denudation*, the GHC represents partially molten lower to middle crust that tunneled southward during the Eocene–Oligocene (Fig. 2B), a process driven by the lateral pressure gradient created by the gravitational potential difference between the Tibetan Plateau and its margins (e.g., Beaumont et al., 2001, 2004; Godin et al., 2006). Subsequently, this channel was exhumed

†E-mail: awebb@lsu.edu

GSA Bulletin; doi: 10.1130/B30626.1; 12 figures; 2 tables; Data Repository item 2012341.

Geological Society of America Bulletin, published online on 21 November 2012 as doi:10.1130/B30626.1

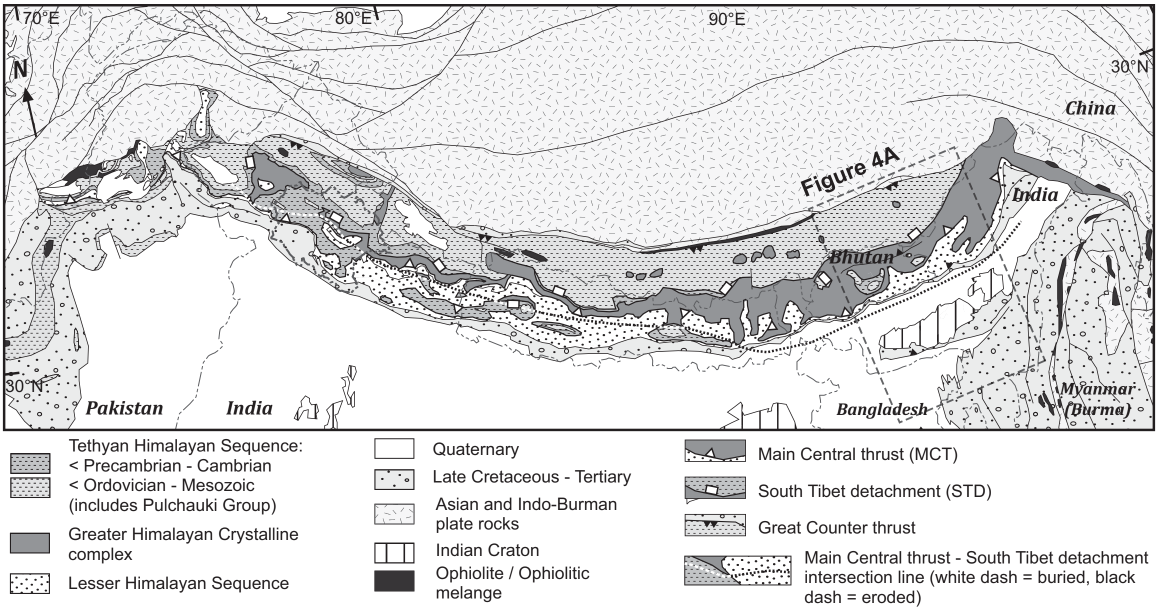

Figure 1. Simplified geological map of the Himalaya, based on Webb et al. (2011b, and references therein).

by enhanced erosion (in response to a climatic change) across a narrow zone where precipitation was focused along the topographic front of the orogen (e.g., Beaumont et al., 2001; Hodges et al., 2001; Clift et al., 2008).

In both wedge extrusion and channel flow–focused denudation models, the Main Central thrust and South Tibet detachment were active, surface-breaching faults during early-middle Miocene GHC emplacement. However, the South Tibet detachment map pattern in the western and Bhutan Himalaya (Yin, 2006) and field, structural, and U-Pb geochronologic studies in the western and central Himalaya (Webb et al., 2007, 2011a, 2011b) indicate that the South Tibet detachment intersects with the Main Central thrust at the leading edge of the GHC. This frontal tip of the GHC is locally preserved; south of this tip, the THS is thrust directly atop the LHS along the Main Central thrust. These observations led to a third kinematic model—that the GHC was emplaced in the early-middle Miocene via *tectonic wedging* (Fig. 2C; Yin, 2006; Webb et al., 2007). Model kinematics are analogous to thrust tectonics of the frontal Canadian Cordillera (Price, 1986): The South Tibet detachment is a backthrust and its motion accommodated GHC emplacement entirely below Earth's surface, with current GHC exposure resulting from subsequent erosion and footwall deformation. Top-to-the-north displacement along the South Tibet detachment is kinematically linked to the north-directed Great Counter thrust system, which juxtaposes THS rocks atop Asian plate–suture-zone rocks to the north (Yin et al., 1994, 1999). Sparse records of alternating top-to-the-north and top-to-the-south shear along the South Tibet detachment (e.g., Hodges et al., 1996; Mukherjee and Koyi, 2010) could be accommodated by slip transfer along a second thrust wedge geometry across the GHC hinterland (Webb et al., 2007).

Some workers have noted similarity between tectonic wedging and channel tunneling processes, as both feature southward motion of the GHC between two subhorizontal shear zones that merge to the south (Kellett and Godin, 2009; Larson et al., 2010a). Modes of inter- and intra-unit shearing may indeed correspond. Nonetheless, the kinematic models of channel flow–focused denudation and tectonic wedging can be distinguished by two criteria: timing and extrusion. In the first model, proposed channel tunneling occurs in the Eocene–Oligocene, preceding the Miocene surface emplacement of the GHC via channel flow coupled to extrusion (e.g., Beaumont et al., 2001; Hodges et al., 2001; Godin et al., 2006). In contrast, proposed tectonic wedging occurred in the Miocene and accomplished emplacement of the GHC at depth, without extrusion (Yin, 2006; Webb et al., 2011b).

A recently proposed GHC emplacement model features southward motion of this unit between two subhorizontal shear zones that intersect to the south in the early Miocene, succeeded by middle Miocene low-angle normal fault development restricted to the crest of the Himalaya (Fig. 2D; Kellett and Grujic, 2012). We term this the *tectonic wedging–low-angle normal fault extrusion* model, favoring the "tectonic wedging" terminology over "channel tunneling" because of the proposed early Miocene timing, and because the leading edge of the modeled GHC was not exhumed by extrusion. Rather, a localized, hinterland portion of the GHC and the early Miocene "lower" South Tibet detachment was extruded between the low-angle normal fault, termed the "upper" South Tibet detachment, and an out-of-sequence thrust (the Kakhtang thrust). Restricted low-angle normal fault motion may be consistent with critical taper theory, as discussed above. Alternatively, such faulting could result from subhorizontal shear tractions applied to the base of the Himalayan brittle upper crust by flow of middle crust (driven southward in response to the lateral pressure gradient that varies with topography; Yin, 1989).

Origins of Himalayan Material

The first model to include non-Indian material in the Himalayan orogen was the early channel flow concept of Nelson et al. (1996). These workers speculated that the GHC might represent Tibetan middle crust that was thickened, partially melted, and extruded southward to the Himalaya during collision. However, most subsequent channel flow–focused denudation models show sufficient northward underthrusting of the suture such that all channelized rock is derived from Indian material (e.g., Beaumont et al., 2004).

Detrital zircon investigation of central Himalaya rocks also suggested a non-Indian GHC origin: differences in detrital zircon age spectra between the GHC and LHS led to the proposal

Geological Society of America Bulletin, published online on 21 November 2012 as doi:10.1130/B30626.1

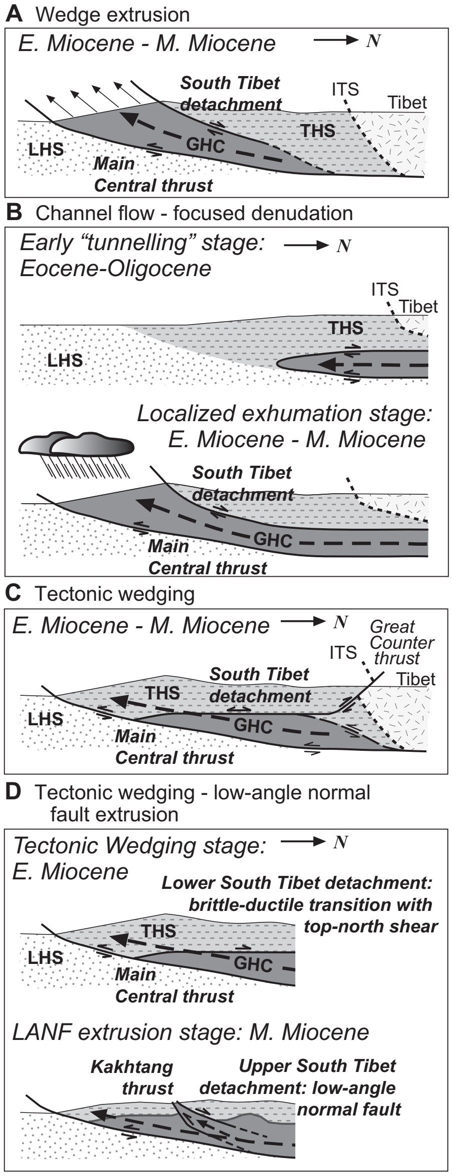

Figure 2. Tectonic models for the emplacement of the Greater Himalayan Crystalline complex (GHC), as described in the text. (A) Wedge extrusion (e.g., Burchfiel and Royden, 1985). (B) Channel flow–focused denudation (e.g., Beaumont et al., 2001). (C) Tectonic wedging (e.g., Webb et al., 2007). (D) Tectonic wedging–low-angle normal fault extrusion (Kellett and Grujic, 2012). ITS—Indus-Tsangpo suture; THS—Tethyan Himalayan Sequence; LHS—Lesser Himalayan Sequence; LANF—low-angle normal fault.

that the GHC was an exotic terrane accreted onto the northern margin of the Indian continent in Cambrian–Ordovician time (DeCelles et al., 2000). Since this work, significant advances have been made in our understanding of key tectonic relationships in the western and eastern Himalaya via systematic field mapping, thermochronological analysis, determination of pressure-temperature (*P-T*) conditions, geochronologic dating of major lithologic units and deformation events, and chronostratigraphic/biostratigraphic work (e.g., Myrow et al., 2003, 2006, 2009, 2010; Hughes et al., 2005, 2011; Grujic et al., 2006; Meyer et al., 2006; Richards et al., 2006; Drukpa et al., 2006; Hollister and Grujic, 2006; Carosi et al., 2006; Webb et al., 2007, 2011a; McQuarrie et al., 2008; Célérier et al., 2009a, 2009b; Kellett et al., 2009, 2010; Long and McQuarrie, 2010; Long et al., 2011a, 2011b; Tobgay et al., 2010; Yin et al., 2006, 2010a, 2010b; Chambers et al., 2009, 2011; McKenzie et al., 2011). Many of these studies indicate potential equivalence of LHS and GHC protoliths. For example, geochronological studies from the western and eastern segments of the Himalayan range demonstrate close correlation of Proterozoic–early Paleozoic stratigraphic units within the THS, GHC, and LHS with the age-equivalent units deposited on the Indian craton (Myrow et al., 2003, 2009, 2010; Richards et al., 2005; McQuarrie et al., 2008; Yin et al., 2010a, 2010b; Long et al., 2011a; Webb et al., 2011a). This result supports the early model that Himalayan materials are derived from Indian basement and cover sequences. Along-strike differences from western and eastern segments to the range center could either be induced by missing stratigraphic sections in the central Himalaya (i.e., Neoproterozoic and Cambrian strata in the LHS in Nepal; Myrow et al., 2003), or by different tectonic processes operating along different parts of the Himalayan orogen.

Recent work suggests that the Himalayan orogen may contain exotic material within its far northeastern part. Late Triassic sedimentary rocks comprise the northern half of the THS in the eastern Himalaya (e.g., Pan et al., 2004). Southward-directed paleoflow indicators, anomalously high ε_{Nd} values, and anomalously young U-Pb/Hf detrital zircon age signals are interpreted to reflect a non-Indian source for these rocks (Li et al., 2003a, 2003b, 2004; Dai et al., 2008; Li et al., 2010). Zircons of appropriate age are not known in India, but they occur in the Lhasa terrane: circa 190–250 Ma inherited zircon occurs in granitoids of the Nyainqentanglha Shan (Kapp et al., 2005); high-pressure metamorphism during intra-Lhasa terrane subduction is dated at ca. 239 Ma (Zeng et al., 2009); amphibolites-facies rocks in the central Lhasa terrane contain ca. 225–213 Ma metamorphic zircon (Dong et al., 2011); and Late Triassic granitoids occur in the eastern Lhasa terrane (Zhu et al., 2011). Three models are proposed (Fig. 3): (1) *Rift-fill*: Detritus was shed from the Lhasa terrane and deposited across both southern Lhasa and northern India during initial continental rifting (Dai et al., 2008). (2) *Lhasa forearc*: Detritus was shed from an arc developed in southern Lhasa in response to northward subduction of the Neotethys Ocean plate (Li et al., 2010). Deposition occurred in the corresponding forearc basin. (3) *Intra-oceanic forearc*: Detritus was shed from an arc developed within the Neotethys Ocean associated with a north-directed subducting plate (Li et al., 2010). Deposition occurred in the corresponding forearc basin. The rift-fill model shows India-Lhasa rifting and drifting initiating in the Late Triassic, whereas the latter two models require India-Lhasa separation prior to the Late Triassic. These latter models also indicate that Late Triassic "THS" rocks were structurally emplaced on India. For the Lhasa forearc model, the predicted structural southern boundary would also represent the Indus-Tsangpo suture (i.e., the suture between India and Asia).

Approach

This study addresses questions of Himalayan material sources by using U-Pb dating of igneous and detrital zircons to establish the lithostratigraphic architecture of the eastern Himalaya. We also present new mapping of the South Tibet detachment along the range crest in southeast Tibet and thereby test models for the assembly of the orogen. The work presented here complements two related studies dealing with the stratigraphic and tectonic evolution of the Shillong Plateau (Yin et al., 2010a) and the structural development of the eastern Himalaya (Yin et al., 2010b).

GEOLOGIC BACKGROUND

Main Himalayan Structures and Units

Models for the origin and assembly of rocks across the Himalayan orogen commonly hinge upon the deformation histories of the LHS, GHC, and THS units and the Main Central thrust and South Tibet detachment structures (Fig. 1). Therefore, it is a significant challenge that the criteria by which these units and structures are defined are not generally agreed upon (e.g., Upreti, 1999; Searle et al., 2008; Long and McQuarrie, 2010). A common approach involves fault-based division of the major units. That is, the LHS, GHC, and THS are separated by the Main Central thrust and South Tibet detachment (e.g., Yin, 2006; Searle et al., 2008). This division requires definitions of the Main Central thrust and South Tibet detachment that are independent of unit descriptions. We follow

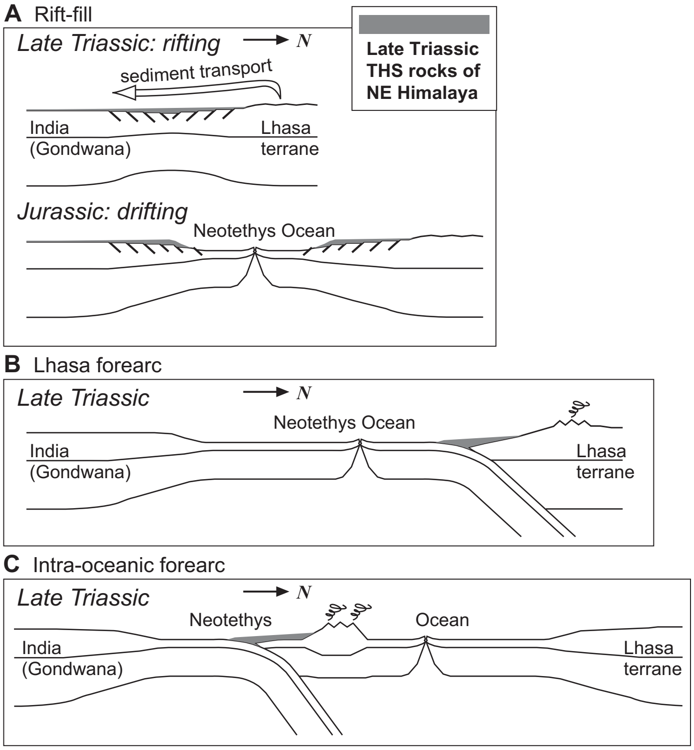

Figure 3. Tectonic models for the deposition of Late Triassic Tethyan Himalayan Sequence (THS) rocks of the northeastern Himalaya. (A) Rift-fill model: derivation from the Lhasa terrane; deposition along the northern Indian margin during initial rifting of Lhasa and India (Dai et al., 2008). (B) Lhasa forearc model: derivation from the Lhasa terrane continental arc; deposition along the Lhasa forearc basin (Li et al., 2010). (C) Intra-oceanic forearc model: derivation from an intra-oceanic arc; deposition in the corresponding forearc basin (Li et al., 2010).

this approach herein, first discussing the Main Central thrust and South Tibet detachment, and then characterizing the tectonic units.

All proposed definitions of the Main Central thrust allow that it occurs in the middle width of the range within a zone of top-to-the-south shear that marks an inverted metamorphic field gradient. Accordingly, a definition based on strain and metamorphism has been proposed: the Main Central thrust would be the complete top-to-the-south shear zone, with all rocks within the shear zone and all rocks within the inverted metamorphic field gradient assigned to the GHC (Searle et al., 2008; Larson and Godin, 2009). This definition has limited utility because the width of the zone of continuous top-to-the-south shearing depends upon the basal transition from distributed to discrete deformation at the scale of field mapping, which is dependent on lithology (Yin et al., 2010b). Rheological variations would therefore locally determine the base of the Main Central thrust shear zone and the GHC. It follows that the timing of Main Central thrust shearing would vary regionally. Also, the lower limit of distributed strain does not always correspond to the lower limit of the inverted metamorphic field gradient (e.g., Vannay and Grasemann, 1998; Webb et al., 2011a).

Main Central thrust definitions that explicitly incorporate timing considerations are more useful for characterizing the kinematic evolution of the orogen (Yin, 2006). Himalayan reconstructions based on field observations, structural geometry, and thermochronology demonstrate that a large thrust sheet was emplaced to the south in the early and middle Miocene, with subsequent south-directed deformation dominated by footwall accretion of smaller horses (e.g., DeCelles et al., 1998, 2001; Robinson et al., 2003, 2006; Bollinger et al., 2004; McQuarrie et al., 2008; Célérier et al., 2009a, 2009b; Herman et al., 2010; Mitra et al., 2010; Long et al., 2011b; Webb et al., 2011a). The two phases of deformation can be locally difficult to distinguish, particularly in the middle width of the range in some arc segments. Nonetheless, across much of the range, the upper thrust sheet is contiguous and deformed into gentle to tight folds, and can therefore be readily differentiated from thrust duplexes below (e.g., Valdiya, 1980; Webb et al., 2011a). Following the works cited already, we interpret the early and middle Miocene thrust underlying this thrust sheet to represent the Main Central thrust, and we provide further description in a companion paper (Yin et al., 2010b).

The South Tibet detachment is distinguished by a zone of top-to-the-north shear, which is uncommon within the largely south-directed Himalayan deformation, occurring within a right-way-up metamorphic field gradient (Burg et al., 1984; Burchfiel et al., 1992). Locally, this structure displays upper, brittle strands (e.g., Hodges et al., 1996; Searle, 2001), whereas a ductile shear zone is present at all known South Tibet detachment exposures (e.g., Carosi et al., 1998; Cottle et al., 2011; Webb et al., 2011a, 2011b; Kellett and Grujic, 2012). The South Tibet detachment was active in the early and middle Miocene (see review by Godin et al., 2006).

The LHS consists largely of Proterozoic to Cambrian sedimentary and metasedimentary strata with small volumes of igneous rocks (e.g., Valdiya, 1980; DeCelles et al., 2001; Long et al., 2011a). Metamorphic conditions are largely greenschist facies but increase to amphibolite facies with increasing proximity to the Main Central thrust (e.g., Beyssac et al., 2004; Martin et al., 2005; Robinson et al., 2006; Célérier et al., 2009a, 2009b; Long et al., 2011c). The GHC is dominated by Late Proterozoic metasedimentary rocks, Cambrian–Ordovician granitoids, and mid-Cenozoic migmatites that display pervasive ductile deformation fabrics and have experienced metamorphism across amphibolite- to granulite-facies conditions (e.g., Le Fort, 1975; Hodges et al., 1996; Vannay and Grasemann, 1998; Vannay et al., 2004; Kohn, 2008; Larson et al., 2010a; Yin et al., 2010b), with eclogite-facies conditions locally preserved (e.g., Corrie et al., 2010; Grujic et al., 2011).

The THS is composed of Late Proterozoic–Phanerozoic (meta-)sedimentary rocks and Cambrian–Ordovician granitoids deformed in an early Cenozoic top-to-the-south fold-and-thrust belt (e.g., Gaetani and Garzanti, 1991; Ratschbacher et al., 1994; Frank et al., 1995; Corfield and Searle, 2000; Aikman et al., 2008). The THS is largely anchizone facies, but grade increases monotonically down section such that the South Tibet detachment commonly displays a <100 °C increase from THS rocks above to ~650–750 °C GHC rocks below (e.g., Schneider and Masch, 1993; Crouzet et al., 2007; Kellett and Grujic, 2012). Unit affiliations of amphibolites-facies rocks within and above the basal

South Tibet detachment are not uniformly assigned. In places where these rocks occur below upper, brittle strands of the South Tibet detachment, they have been variably interpreted as GHC (e.g., Larson et al., 2010a), THS (Webb et al., 2011b), or an intermediate unit (Jessup et al., 2008). These horse rocks may be only modestly offset from contiguous THS rocks because in regions where the South Tibet detachment is a single shear zone, the up-section decrease in maximum metamorphic temperatures from ~650 °C to ~350 °C occurs across 1–5 km of structural thickness above and/or within the shear zone (Grujic et al., 2002; Chambers et al., 2009; Kellett et al., 2009, 2010; Cottle et al., 2011; Webb et al., 2011a; Kellett and Grujic, 2012). That is, the thermal pattern from the basal South Tibet detachment to the anchizone facies rocks high above is not changed by the presence or absence of the brittle, upper strands.

Bhutan Himalaya

The Bhutan Himalaya is distinguished from the rest of the range by isolated southern exposures of THS rocks that occur as close as ~2 km north of the Main Central thrust (Figs. 1 and 4; e.g., Gansser, 1983; Bhargava, 1995). Geological investigations generally reveal that these THS rocks comprise klippen of the South Tibet detachment above the GHC (e.g., Grujic et al., 2002; McQuarrie et al., 2008; Kellett et al., 2009, 2010; Chambers et al., 2011). Depositional contacts between THS and GHC rocks were also interpreted by Long and McQuarrie (2010) in south-central Bhutan, although this interpretation is controversial (cf. Webb et al., 2011b; Greenwood et al., 2011).

The LHS is dominated by garnet-bearing schist in the Jaishidanda Formation, quartzite and phyllite in the Daling-Shumar Group, quartzite and minor carbonates in the Baxa Formation, and sandstones and shales of the Gondwanan succession (Gansser, 1983; Bhargava, 1995; McQuarrie et al., 2008). Detrital zircon U-Pb geochronology yields maximum depositional ages of ca. 475–500 Ma for the Jaishidanda Formation (and loosely correlative Paro Formation), ca. 1.8–1.9 Ga for the Daling-Shumar Group, ca. 520 Ma for the Baxa Formation, and ca. 390 Ma for the Gondwanan succession (and correlative Diuri Formation; Richards et al., 2006; McQuarrie et al., 2008; Tobgay et al., 2010; Long et al., 2011a). Numerous granitic gneisses are exposed as lenses in map view and are interlayered with LHS metasedimentary rocks. These include the Jhumo Ri granitic gneiss of Jangpangi (1974) and the Gachhang granitic gneiss of Ray et al. (1989), which yielded Rb-Sr ages of ca. 1.1 Ga (Bhagava, 1995) and U-Pb zircon ages of ca. 1.76 Ga (Daniel et al., 2003), respectively. Similar orthogneiss crosscuts bedding in the Daling-Shumar Group and yields crystallization ages of ca. 1.8–1.9 Ga (Long et al., 2011a). The Jaishidanda Formation schist unit directly below the lithological Main Central thrust experienced peak metamorphism at 650–675 °C and 9–13 kbar during 18–22 Ma (Daniel et al., 2003).

The GHC in Bhutan consists of paragneiss, orthogneiss, migmatite, and Tertiary leucogranite (Gansser, 1983). Detrital zircon U-Pb geochronology yields maximum depositional ages ranging from ca. 460 Ma to ca. 0.9 Ga for proposed GHC samples in central Bhutan (Long and McQuarrie, 2010), but these are alternately considered THS rocks (e.g., Kellett et al., 2009; Webb et al., 2011b; Greenwood et al., 2011). In eastern Bhutan, an 825 Ma orthogneiss intrudes a quartzite unit in the GHC, which yields U-Pb detrital zircon ages between 980 and 1820 Ma (Richards et al., 2006). Kyanite-bearing migmatites in eastern Bhutan experienced peak *P-T* conditions of ~750–800 °C and 10–14 kbar at ca. 18 Ma, followed by retrograde metamorphism under *P-T* conditions of 500–600 °C and ~5 kbar, which was accompanied by 13 Ma leucogranite crystallization and a cooling event at 14–11 Ma in the Main Central thrust zone (Stüwe and Foster, 2001; Daniel et al., 2003). Peak metamorphic temperatures across the bulk of the debated GHC/THS rocks of central Bhutan are ~200–300 °C lower, ranging from ~475 °C to ~675 °C (Long and McQuarrie, 2010). A recent discovery of Miocene granulitized eclogites in the northwest Bhutan GHC further expands the range of known GHC *P-T* conditions here (Grujic et al., 2011; Warren et al., 2011).

The THS in Bhutan is exposed mostly in the South Tibet detachment klippen and consists of the garnet-bearing pelitic rocks and quartzite of the Neoproterozoic(-Ordovician?) Chekha Formation, rhyolite-dacite flows of the Singhi Formation, and quartz arenite of the Deshichiling Formation, all overlain by Cambrian–Jurassic strata (Gansser, 1983; Tangri et al., 2003; Long and McQuarrie, 2010; Hughes et al., 2011; McKenzie et al., 2011). The Chekha Formation is generally considered to form the oldest, deepest unit observed in the South Tibet detachment hanging wall, but its regional distribution is uncertain. Recent work documents both ca. 493 Ma age-diagnostic trilobites in rocks above interpreted Chekha Formation strata in central Bhutan (Hughes et al., 2011) and a youngest detrital zircon age peak of ca. 460 Ma from interpreted Chekha Formation rocks of south-central Bhutan (Long and McQuarrie, 2010). New regional stratigraphic determinations appear warranted.

Southeast Tibet

Southeast Tibet, north of the Himalayan crest, exposes THS rocks (Figs. 1, 4, and 5A). They are dominantly Triassic, Jurassic, and Cretaceous flysch deposits bounded by the south-dipping Renbu-Zedong thrust zone (alternatively termed the Great Counter thrust) in the north and the north-dipping South Tibet detachment in the south (Fig. 5A; Pan et al., 2004). Major structures in the area include the Yalaxianbo gneiss dome, the Lhunze thrust, and the Lhamei thrust. The Yalaxianbo gneiss dome exposes high-grade gneisses and is bounded by a low-angle ductile shear zone with both top-to-the-north and top-to-the-south sense of shear indicators (Pan et al., 2004; Aikman, 2007). Doming occurred during or after the middle Miocene, as recorded by tilting of fabrics developed in the early and middle Miocene (Antolín et al., 2010).

North of the Lhunze thrust, axial-planar cleavage is well developed in the Late Triassic strata and in many places replaces the original bedding (Yin et al., 1999; Antolín et al., 2010, 2011; Dunkl et al., 2011). Significant shortening of these rocks was accomplished prior to and at ca. 44 Ma, as constrained by U-Pb ages of undeformed granite crosscutting cleavage fabrics (Aikman et al., 2008) and K-Ar ages of metamorphic muscovites (Dunkl et al., 2011). As discussed earlier herein, the Late Triassic rocks of southeast Tibet are probably not sourced from India (Dai et al., 2008; Li et al., 2010). Existing sedimentologic observations from these strata (i.e., southward paleocurrent directions) are consistent with a northern source (Li et al., 2003a, 2003b, 2004). Detrital zircon U-Pb geochronology yields age peaks ranging from ca. 200 Ma to ca. 3 Ga for the Triassic strata; the youngest ages (ca. 224–266 Ma) yield juvenile $\varepsilon_{Hf(T)}$ values (5.5–13.5; Aikman et al., 2008; Li et al., 2010). Late Triassic strata have $\varepsilon_{Nd(0)}$ values between –5.42 and –9.76 (Dai et al., 2008; see sample distributions and corresponding Nd isotope values in Fig. 5A). In contrast, Cretaceous samples to the south of the Lhamei thrust yield $\varepsilon_{Nd(0)}$ values between –16.74 and –18.00, consistent with an Indian source, with one exception (–7.95) discussed later herein (Dai et al., 2008).

South of the Lhamei thrust, Early Cretaceous strata form the immediate hanging wall of the South Tibet detachment (Pan et al., 2004). The Early Cretaceous age for these rocks is inferred via lithologic correlation to similar, dated strata ~100 km to the northwest (Zhu et al., 2008) and Cretaceous fossils in similar rocks to the west (Pan et al., 2004; Dai et al., 2008). The juxtaposition of Cretaceous strata against the South

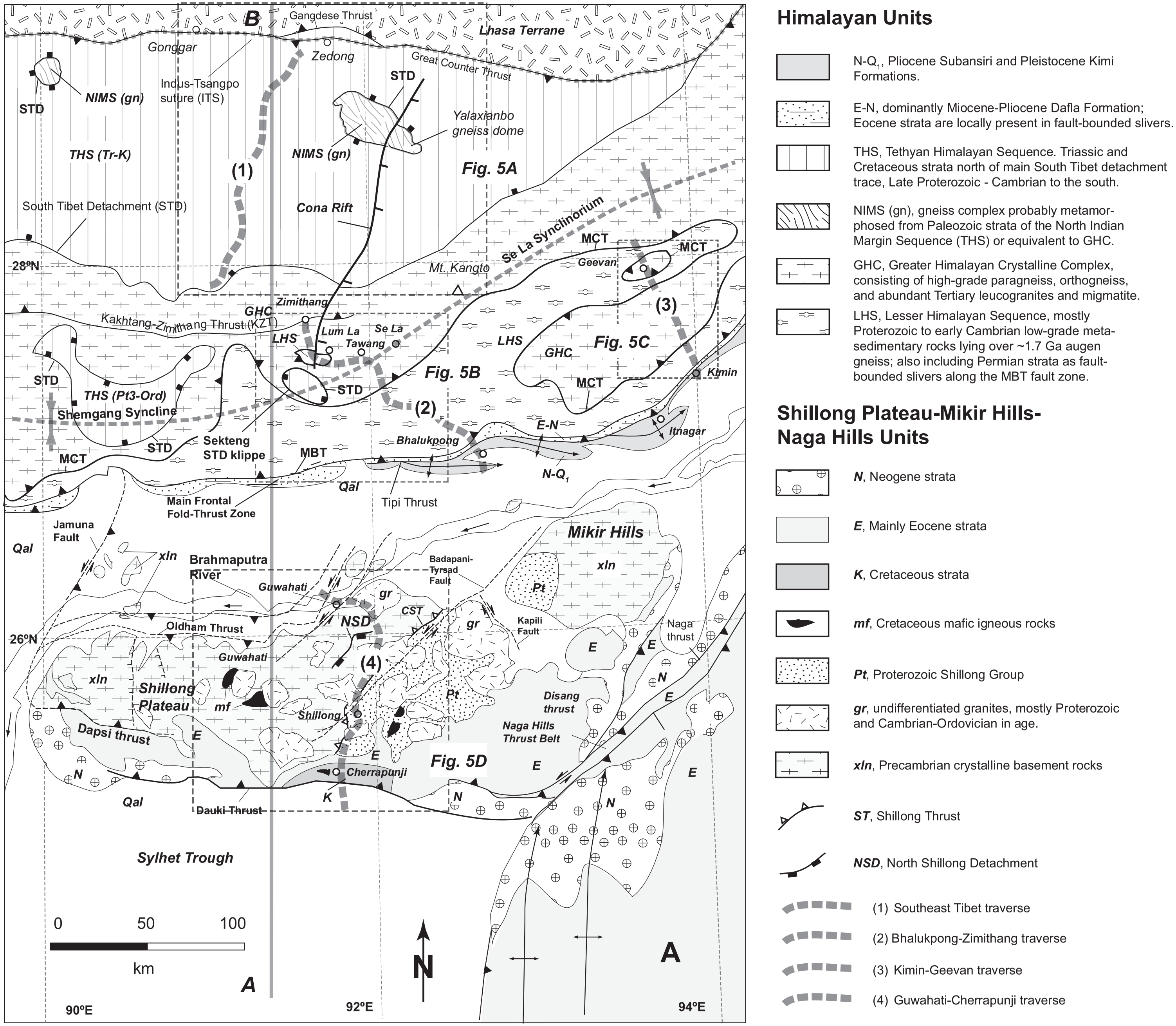

Figure 4 (*on this and following page*). (A) Schematic geological map of the eastern Himalaya and northeastern Indian craton, modified from Yin et al. (2010a, 2010b). See Figure 1 for location. Locations of regional maps for sampled regions (Fig. 5) are indicated. (B) Schematic regional geologic cross section across the eastern Himalaya and the Shillong Plateau in NE India, modified from Yin et al. (2010a). NIMS—North Indian margin sequence; MBT—Main Boundary thrust; MCT—Main Central thrust.

Geological Society of America Bulletin, published online on 21 November 2012 as doi:10.1130/B30626.1

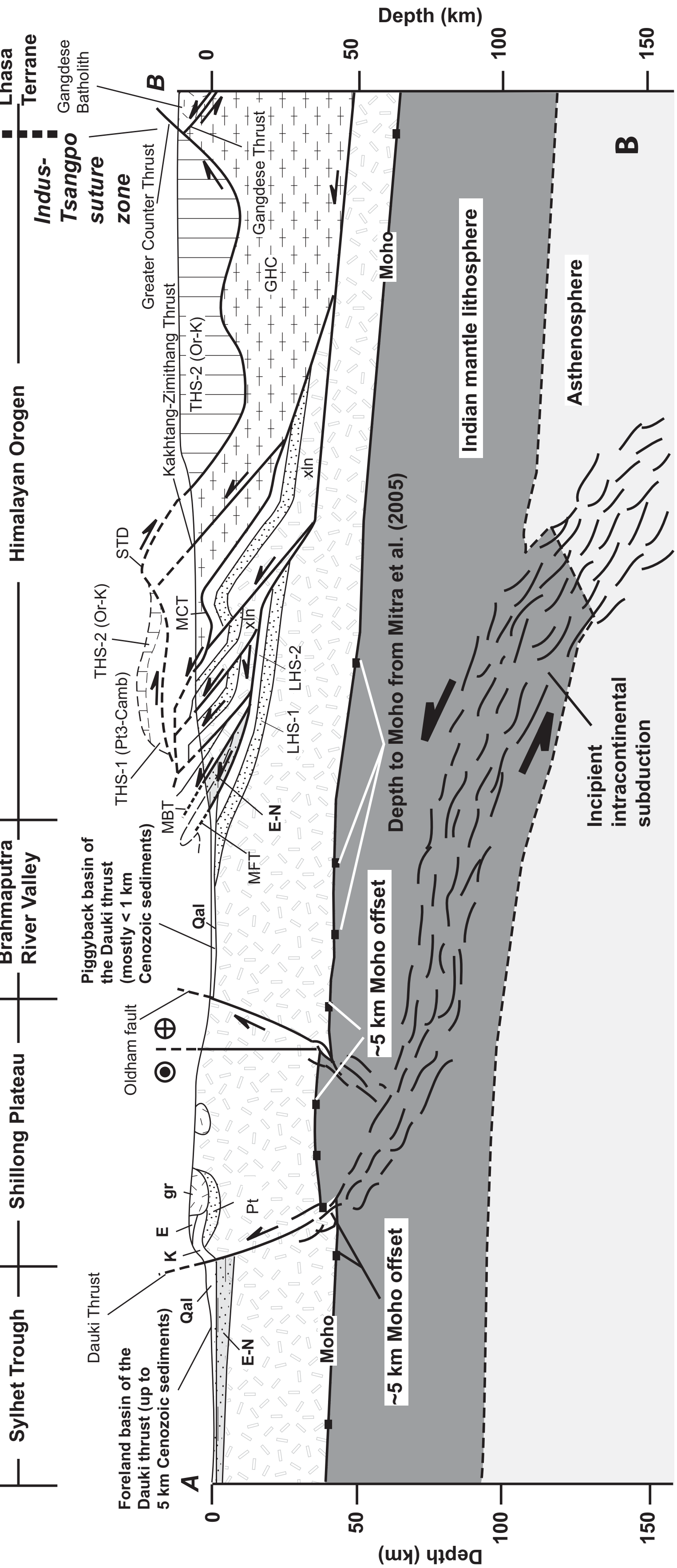

Figure 4 (*continued*).

Tibet detachment contrasts sharply to the presence of the Proterozoic Chekha Formation directly above this structure in southern Bhutan (Grujic et al., 2002), suggesting that the South Tibet detachment cuts up section in its northward transport direction. On the other hand, the rocks of the immediate South Tibet detachment hanging wall in southeast Tibet are transposed by isoclinal folding, and their stratigraphy is poorly constrained (Dai et al., 2008). An exceptionally low $\varepsilon_{Nd(0)}$ value was obtained from the structurally deepest THS sample analyzed by Dai et al. (2008), yielding a value (–7.95) consistent with the range for Late Triassic samples. Therefore, future stratigraphic studies may better delineate the possible up-section cutting along the South Tibet detachment here.

Intermediate to mafic shallow intrusive and volcanic rocks occur across southeast Tibet (e.g., Zhu et al., 2005, 2007, 2008). These occur as 145–130 Ma sills and dikes crosscutting Early Cretaceous rocks south of the Lhamei thrust, where they are interpreted as initial magmatic products of the Kerguelen plume (Zhu et al., 2008). Similar rocks are folded with Late Triassic strata to the north (Antolín et al., 2010). The age of the igneous rocks in the Late Triassic strata is uncertain, although Dunkl et al. (2011) interpreted Early Cretaceous illite growth (constrained by K-Ar geochronology) in adjacent metapelites as indicative of similar 145–130 Ma igneous crystallization. If correct, this interpretation implies that the Late Triassic strata were proximal to the Early Cretaceous strata at 145–130 Ma, despite the apparently exotic source of the former rocks.

Arunachal Himalaya

The Arunachal Himalaya only exposes the LHS and GHC units, with the THS exposed north of the Himalayan crest in southeast Tibet (Figs. 1, 4, 5B, and 5C). Yin et al. (2006) showed that a quartz arenite unit in the LHS contains detrital zircon with ages younger than ca. 960 Ma. The arenite and its interbedded phyllite constitute the Proterozoic Rupa Group of Kumar (1997). Orthogneiss in the LHS yields U-Pb ages of ca. 1.74 Ga (Yin et al., 2010b) and Rb-Sr ages of 1.5–1.9 Ga (Dikshitulu et al., 1995). The carbonate-bearing Baxa Formation of Tewari (2001), equivalent to the uppermost part of the Rupa Group of Kumar (1997), contains latest Proterozoic to Early Cambrian fossils. The GHC in Arunachal contains orthogneisses that yield U-Pb zircon ages of ca. 1.74 Ga, ca. 878 Ma, and ca. 500 Ma, all of which were also found in the Main Central thrust footwall rocks and in the Indian craton (Yin et al., 2010a, 2010b).

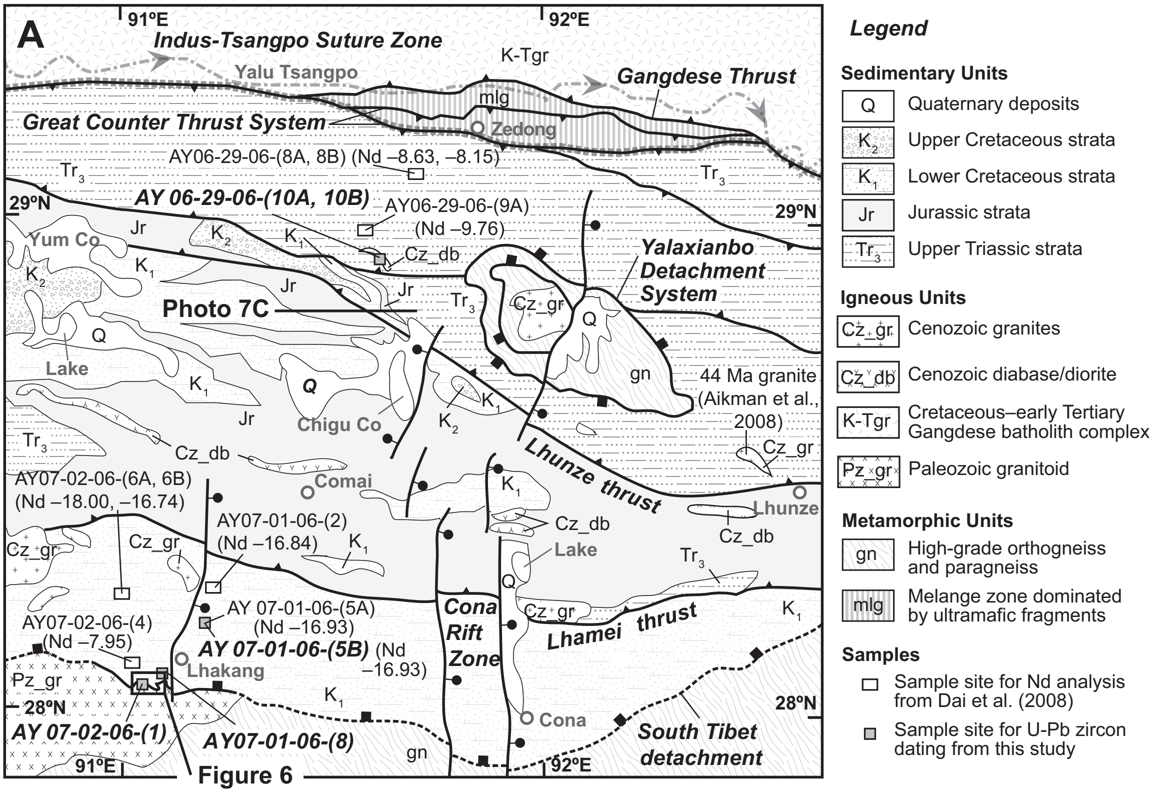

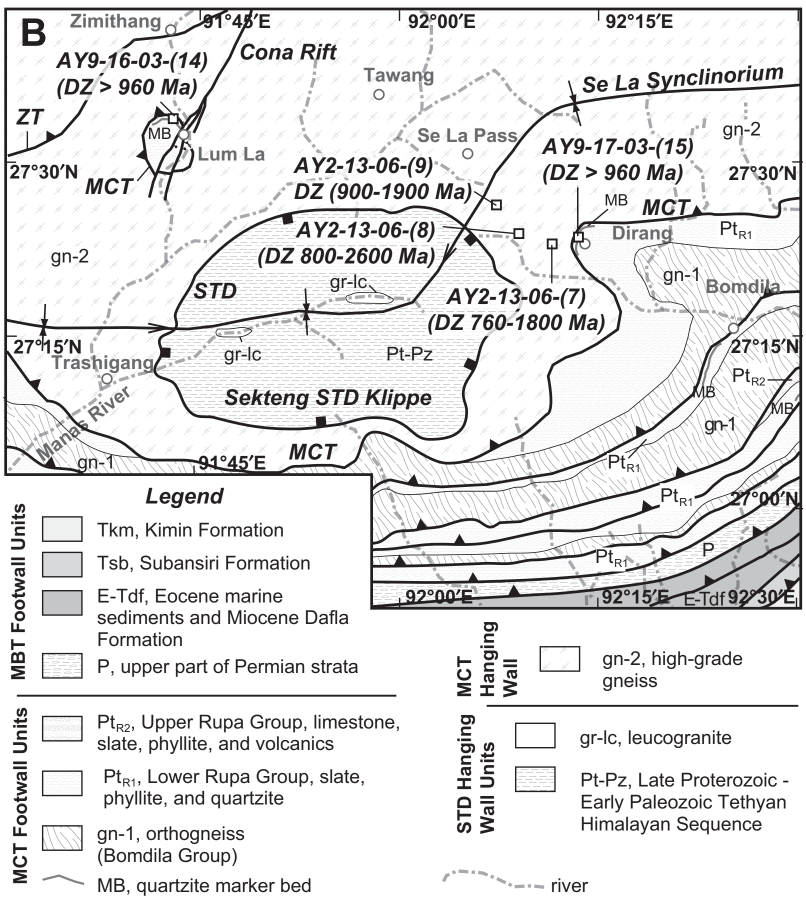

Figure 5 (*on this and following page*). (A) Geological map of southeast Tibet based on Yin et al. (1994, 1999), Harrison et al. (2000), Pan et al. (2004), Aikman et al. (2008), and our work. Location of Figure 6 map is indicated. (B) Geological map of Bhalukpong traverse region, modified from Yin et al. (2010b). (C) Geological map of Kimin traverse region, modified from Yin et al. (2010b). (D) Geological map of central Shillong Plateau, modified from Yin et al. (2010a). MCT—Main Central thrust; STD—South Tibet Detachment.

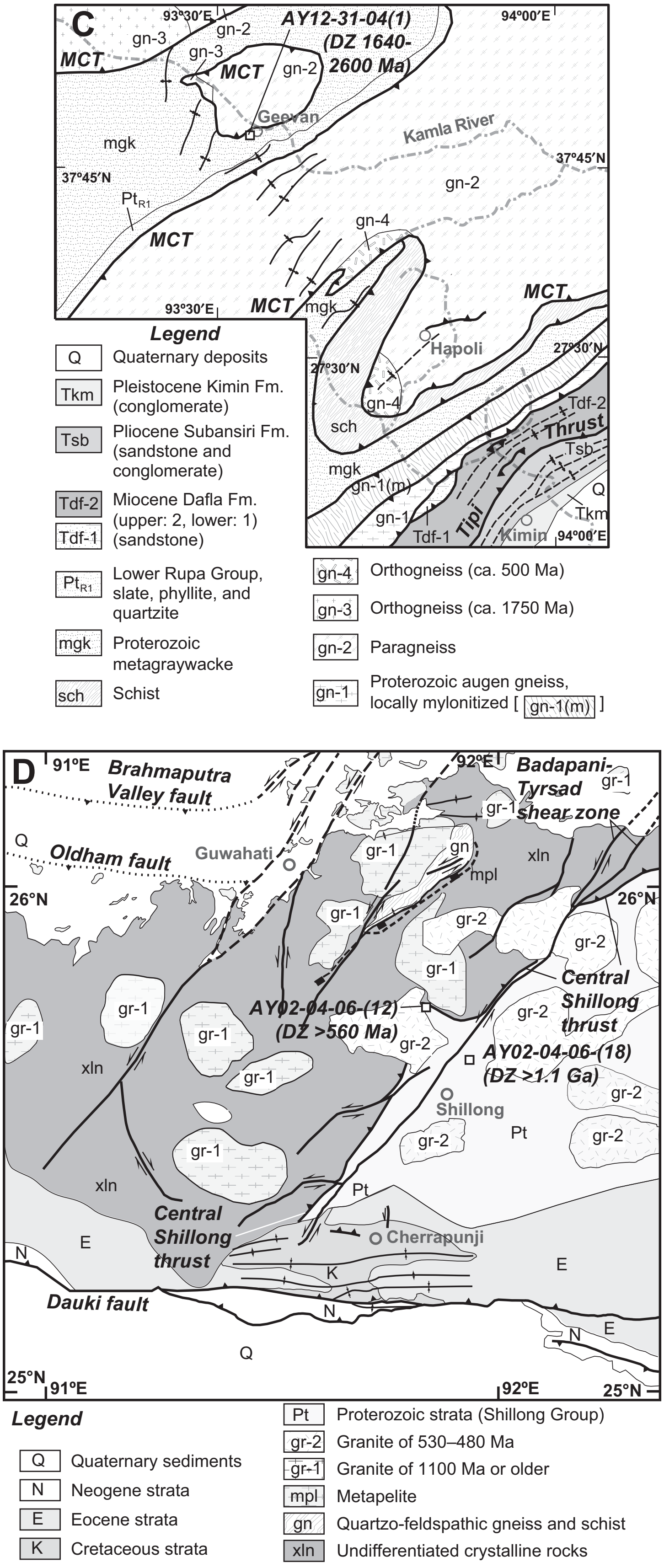

Figure 5 (***continued***).

Shillong Plateau and NE Indian Craton

The Shillong Plateau is a Cenozoic pop-up structure (Bilham and England, 2001; Gupta and Sen, 1988; Rajendran et al., 2004; Biswas and Grasemann, 2005; Biswas et al., 2007), and it exposes a crystalline basement overlain by Proterozoic to Neogene sedimentary strata (Das Gupta and Biswas, 2000) (Figs. 1, 4, and 5D). The basement is composed of sillimanite-bearing paragneiss, amphibolites, banded iron formations, granulites, and orthogneiss (e.g., Ghosh et al., 2005). The basement is overlain by the Proterozoic Shillong Group, consisting of quartz arenite, sandstone, and phyllite; all of these units experienced multiple phases of folding and locally lower-greenschist-facies metamorphism (Ghosh et al., 1994; Mitra and Mitra, 2001). The Shillong Plateau and its neighboring region are also extensively intruded by granitoids that yield Rb-Sr whole-rock isochron ages of ca. 1700 Ma, ca. 1400 Ma, ca. 1100 Ma, ca. 800 Ma, and ca. 700 Ma (Crawford, 1969; van Breemen et al., 1989; Ghosh et al., 1991, 1994, 2005). Some of the granitoids were recently dated using the U-Pb zircon method, which yields three groups of ages at 1600 ± 50 Ma, 1100 ± 50 Ma, and 500 ± 30 Ma (Yin et al., 2010a). The youngest granitoids intrude into the Shillong Group, requiring part of the Shillong Group to have been deposited prior to ca. 500 Ma (Yin et al., 2010a). Two samples from the Shillong Group yield detrital zircon age distributions dominated by Proterozoic ages, with dominant age clusters at 900–1150 Ma and 1450–1850 Ma for one sample and 1100–1250 Ma and 1500–1750 Ma for the second sample (Yin et al., 2010a). The youngest ages suggest that parts of the Shillong Group were deposited after ca. 560 Ma and ca. 1100 Ma.

STRUCTURAL GEOLOGY OF THE SOUTH TIBET DETACHMENT NEAR LHAKANG, SOUTHEAST TIBET

The South Tibet detachment is exposed ~10 km southwest of Lhakang as a distributed shear zone with a minimum thickness of 200 m (Fig. 6). As the fault is located along the international border between Bhutan and China, we did not observe the base of the shear zone. The shear zone is primarily developed across a coarse-grained augen gneiss unit dominated by large K-feldspar phenocrysts, 0.5–3 cm in diameter, and plagioclase with minor muscovite, biotite, hornblende, and quartz. The shear zone also involves minor amounts of garnet schist and quartzite. Rocks above the shear zone include both biotite schist and garnet schist. The garnet

Geological Society of America Bulletin, published online on 21 November 2012 as doi:10.1130/B30626.1

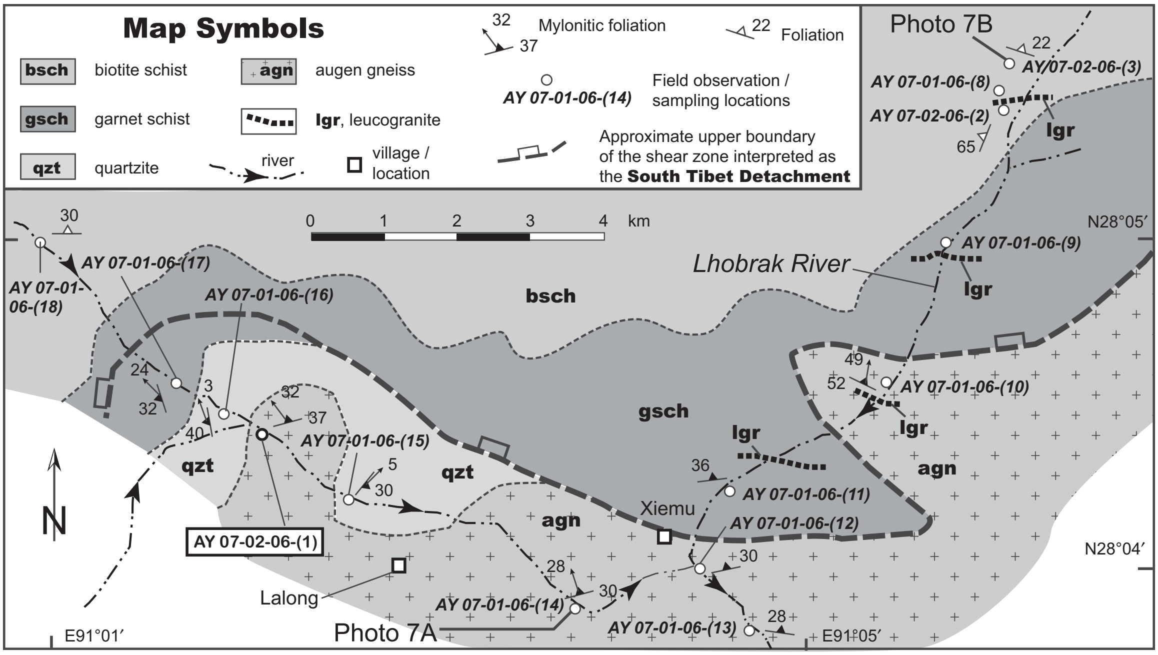

Figure 6. Geological map of the South Tibet detachment to the southwest of Lhakang, southeast Tibet. Location noted in Figure 5A.

schist unit is intruded by both deformed and undeformed leucogranite sills. The leucogranites are fine-grained, containing quartz, muscovite, and tourmaline, ± garnet. They occur as dikes and sills with maximum widths of a few meters. Farther to the north, ~10–15 km north of the shear zone, the metamorphic grade decreases from biotite schist to phyllitic schist, phyllite, and metagraywackes. In general, metamorphic grade across the mapped shear zone and hanging wall decreases gradually with increasing structural elevation.

The augen gneiss unit displays well-developed mylonitic fabrics with dominantly top-to-the-north sense of shear (Fig. 7A). Mylonitic fabrics are not distributed uniformly in the augen gneiss unit, and in places they are completely lacking in regions bounded by sheared rocks. Similar mylonitic fabrics and extensional boudinage are developed across the shear zone quartzite and garnet schist. There is no sharp contact marking the upper limit of the shear zone. For example, in some locations above the mapped upper limit, asymmetric folds that deform leucogranites also indicate top-to-the-north sense of shear (Fig. 7B).

SAMPLE LOCATIONS AND LOCAL GEOLOGICAL SETTINGS

In this study, we analyzed a total of eight samples using U-Pb zircon geochronology, six from sedimentary rocks and paragneiss units for detrital zircon analysis and two samples from plutonic bodies. Samples were collected from southeast Tibet, far western Arunachal (Bhalukpong-Tawang traverse of Yin et al., 2010b), and central western Arunachal (Kimin traverse of Yin et al., 2010b) (Fig. 4).

Detrital zircon sample AY06–29–06–10A was collected from intensely folded upper Triassic turbidite strata of the Tethyan Himalayan Sequence in southeast Tibet (Fig. 5A). The strata where sample AY06–29–06–10A was collected are intruded by northwest-trending diabase dikes (see Fig. 7C for a similar relationship exposed to the south). Sample AY06–29–06–10B was collected from a diabase dike to constrain the age of igneous emplacement (Fig. 5A).

Sample AY07–01–06–5B was collected from Cretaceous strata exposed between the Lhamei thrust and the South Tibet detachment (Fig. 5A; Pan et al., 2004). To our knowledge, Cretaceous strata are the youngest stratigraphic unit that the South Tibet detachment cuts in its hanging wall (see prior review of southeast Tibet geology; Yin, 2006; Yin et al., 2010b). This relationship in southeast Tibet contrasts with the typical relationship of the South Tibet detachment, which places Cambrian–Ordovician or Neoproterozoic strata in its hanging wall in the central Himalaya (Burchfiel et al., 1992) and in the Bhutan Himalaya directly south of this sample location (e.g., Grujic et al., 2002; McQuarrie et al., 2008; Hughes et al., 2011; McKenzie et al., 2011). Despite its young age, Cretaceous rocks where sample AY07–01–06–5B was collected are metamorphosed into biotite schist. We also collected augen gneiss sample AY07–02–06–1 from within the South Tibet detachment shear zone on the Bhutan-Tibet border (Fig. 6). It is mylonitized and displays a top-to-the-north sense of shear.

Three samples were collected from the Bhalukpong-Tawang traverse. Samples AY02–13–06–7, AY02–13–06–8, and AY02–13–06–9B were collected systematically from lower to higher structural levels in a north-dipping section of the GHC in the Main Central thrust hanging wall (Fig. 5B). Samples AY02–13–06–7 and AY02–13–06–9B were collected from quartzofeldspathic biotite gneiss, whereas sample AY02–13–06–8 was collected from a garnet biotite gneiss unit.

Sample 12–31–04–1 was collected from the Lesser Himalayan Sequence directly below the Main Central thrust fault in the Kimin area (Fig. 5C). The composition of this sample is an arkosic sandstone. The arkosic sandstone is interlayered with phyllite, both of which are folded with well-developed cleavage. Intense isoclinal folding in the phyllite units has mostly transposed the original bedding, and the newly developed cleavage itself is broadly folded (Fig. 6; Yin et al., 2010b). Yin et al. (2010b) referred to this sequence as metagraywacke and assigned it to the lower unit of the Proterozoic Rupa Group.

Geological Society of America Bulletin, published online on 21 November 2012 as doi:10.1130/B30626.1

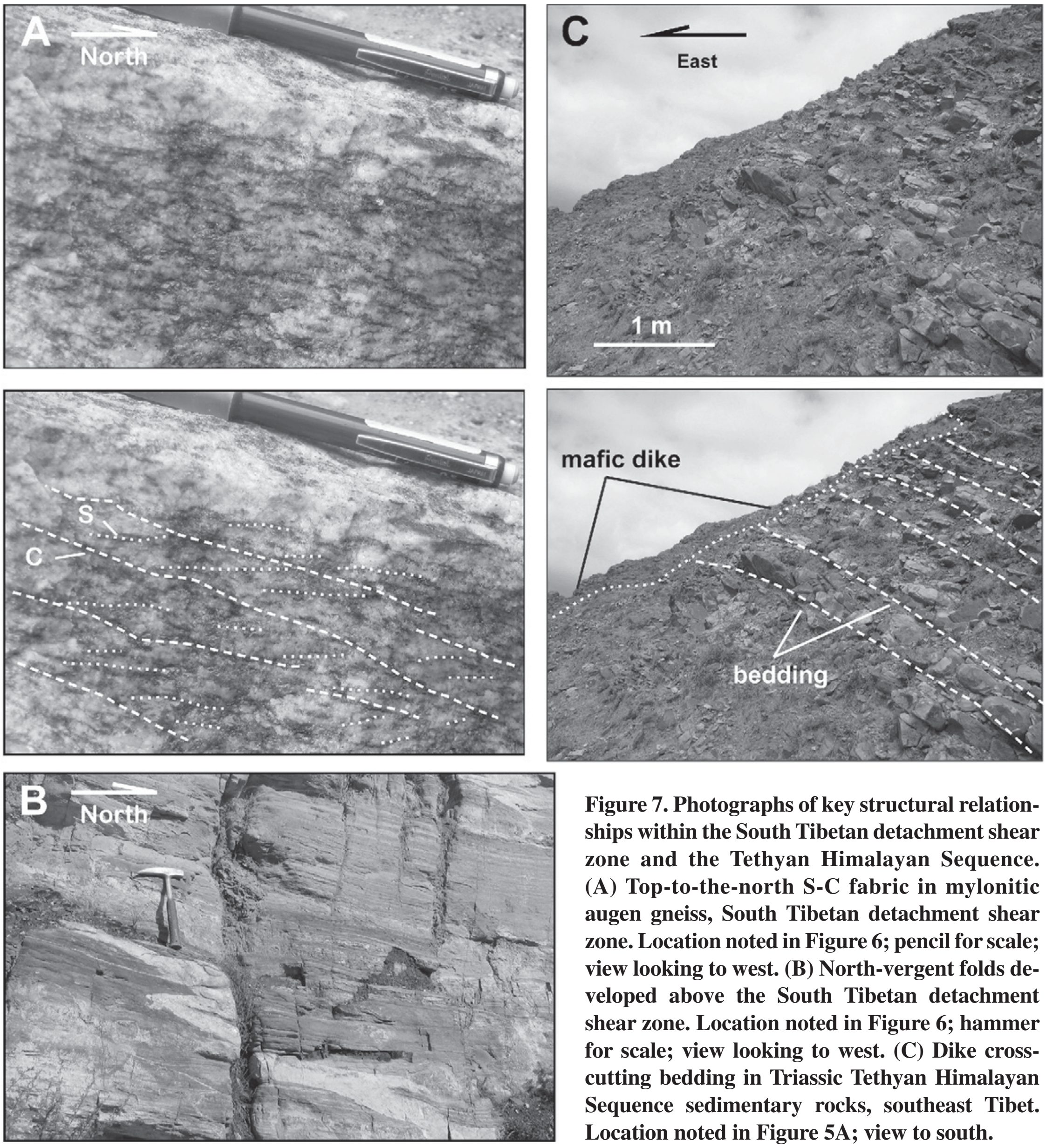

Figure 7. Photographs of key structural relationships within the South Tibetan detachment shear zone and the Tethyan Himalayan Sequence. (A) Top-to-the-north S-C fabric in mylonitic augen gneiss, South Tibetan detachment shear zone. Location noted in Figure 6; pencil for scale; view looking to west. (B) North-vergent folds developed above the South Tibetan detachment shear zone. Location noted in Figure 6; hammer for scale; view looking to west. (C) Dike cross-cutting bedding in Triassic Tethyan Himalayan Sequence sedimentary rocks, southeast Tibet. Location noted in Figure 5A; view to south.

U-Pb ZIRCON GEOCHRONOLOGY

Methods

U-Pb measurements were undertaken using laser ablation–multicollector–inductively coupled plasma–mass spectrometry (LA-MC-ICP-MS; methods following Gehrels et al., 2006) at the Arizona LaserChron Center. For construction of relative probability distributions, we generally follow the "best age" approach common to detrital zircon studies: For ages older than 1000 Ma, we use the $^{207}Pb/^{206}Pb$ age, whereas for ages younger than 1000 Ma, we use the $^{206}Pb/^{238}U$ age. However, our three GHC samples have a few, discordant ages slightly younger than 1000 Ma. For these samples, we use $^{207}Pb/^{206}Pb$ results for all analyses. We also obtained U-Pb ages for two igneous samples using the CAMECA IMS 1270 ion microprobe at The University of California–Los Angeles. The analytical procedures are described in detail in Schmitt et al. (2003). Uncertainties discussed herein are quoted as ±1σ standard deviations, except where otherwise noted.

Detrital Zircon Spectra of the THS Samples

To determine and differentiate the provenance of Triassic and Cretaceous THS strata, we analyzed 92 zircon grains from a Late Triassic turbidite sequence north of the Lhunze thrust (sample AY 06–29–06 10A). We also analyzed 83 zircon grains from Early Cretaceous strata south of the Lhamei thrust (sample AY 07–01–06 5B; locations shown in Fig. 5A). Analyses for both samples are dominantly concordant for ages younger than 1200 Ma and discordant for ages older than 1200 Ma (see GSA Data Repository Supplementary File 1[1]). Both

[1]GSA Data Repository item 2012341, Supplementary File 1. Detrital zircon U-Pb results: A. Concordia diagrams. B. Age histograms with relative probability curves. C. Cumulative probability curves. D. Tabulated data. Supplementary File 2. Cathodoluminesence (CL) images of analyzed zircons from igneous samples, with analysis locations indicated, is available at http://www.geosociety.org/pubs/ft2012.htm or by request to editing@geosociety.org.

samples feature a large variety of ages that range from ca. 200 Ma to ca. 3500 Ma (Fig. 8). Results are concentrated in the Cambrian, Late Proterozoic, and to a lesser extent the late Middle Proterozoic. Results from the two samples can be distinguished because (1) the Triassic sample has a well-defined age peak at ca. 570 Ma, whereas the Cretaceous sample lacks well-defined age peaks, and (2) the Triassic sample has an age cluster between 220 Ma and 280 Ma with a peak at ca. 250 Ma, whereas the Cretaceous sample has only three scattered ages younger than ca. 500 Ma. Comparison of the spectra using the Kolmogorov-Smirnov statistic (see Press et al., 2007; Fletcher et al., 2007) indicates that the age distributions are distinguishable at the 95% confidence level (Table 1).

Detrital Zircon Spectra of the GHC Samples

We acquired U-Pb detrital zircon age data from three GHC paragneiss samples: 108 analyses for AY 02–13–06 7 at the lowest structural level, 112 analyses of AY 02–13–06 8 in the middle level, and 108 analyses of AY 02–13–06 9B at the highest level (see Fig. 5B for sample locations). Results are dominantly concordant to weakly discordant, with a main age range spanning from the Middle Proterozoic through the early Late Proterozoic, with a few older ages (Fig. 8).

Samples AY 02–13–06 7 and AY 02–13–06 9B yield similar age populations, with similar ranges and moderately well-defined peaks at ca. 1000 Ma, ca. 1150 Ma, and ca. 1380 Ma. The Kolmogorov-Smirnov statistic indicates that these two age distributions are indistinguishable at the 95% confidence level (Table 1). Interestingly, we note that the two samples also have very similar lithology. This may indicate that the two units have been duplicated tectonically either by thrusting or folding.

Sample AY 02–13–06 8 features broadly similar age peaks in comparison with the other two samples collected from the GHC in the Bhalukpong-Tawang traverse, but it has an additional, well-defined youngest age peak at ca. 830 Ma. This indicates a maximum depositional age that is ~170 m.y. younger than those of the other two samples (Fig. 8). The Kolmogorov-Smirnov statistic indicates that AY 02–13–06 8 results represent a distinct age distribution versus the other two GHC samples (Table 1).

Detrital Zircon Spectra of the LHS Samples

Detrital zircon age spectra of Yin et al. (2006) for two Lesser Himalayan Sequence samples (AY 09–16–03 14A, AY 9–17–03 15) along the Bhalukpong-Tawang traverse (Fig. 5B) are indistinguishable at the 95% confidence level (Table 1): they are dominated by late Early Proterozoic through Middle Proterozoic ages with sparse ages older than 1900 Ma. These age ranges are similar to the age distributions for Bhalukpong GHC samples AY 02–13–06 7 and AY 02–13–06 9B (Fig. 8). Indeed, the Kolmogorov-Smirnov statistic indicates that GHC sample AY 02–13–06 7 is indistinguishable from sample AY 09–17–03 15 at the 95% confidence level (Table 1).

In contrast, new results from sample AY 12–31–04 1 of a LHS graywacke unit along the Kimin traverse (Fig. 5C) reveal an age population that is distinct from the Bhalukpong GHC

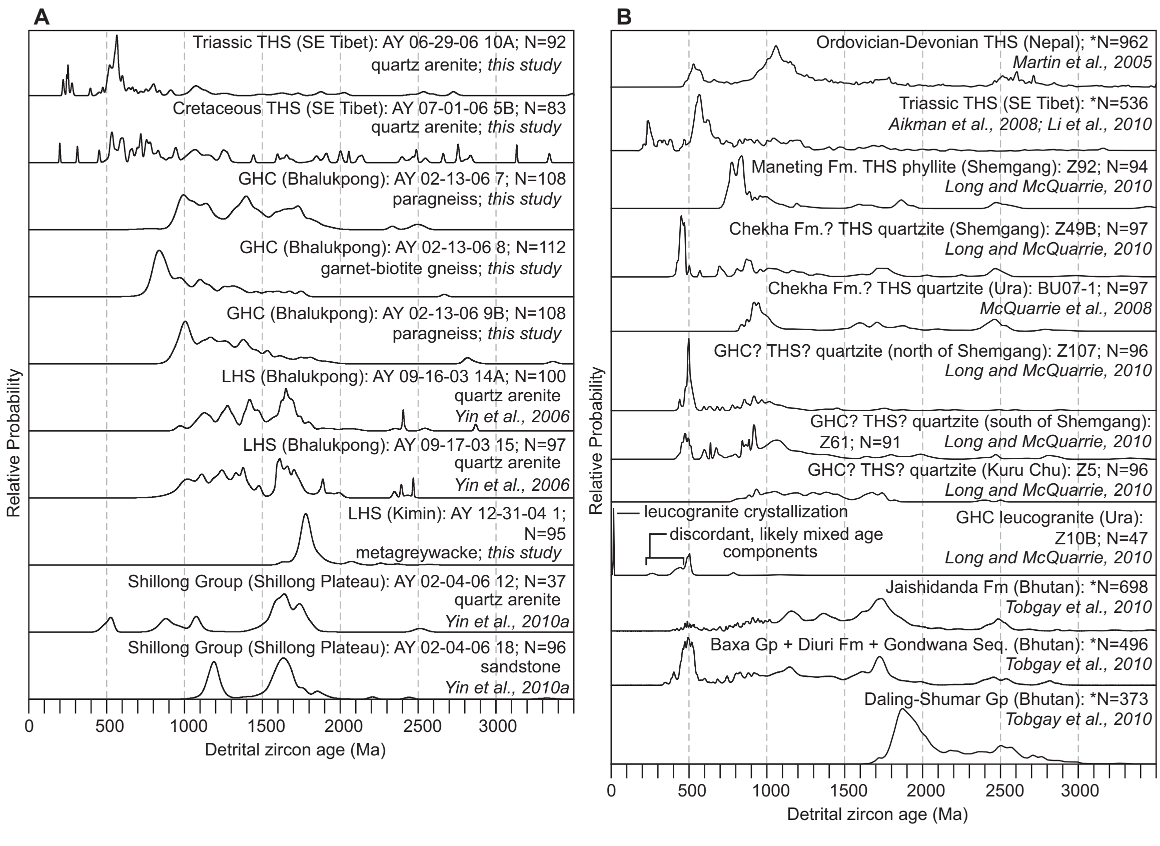

Figure 8. (A) Probability density plots (0–3500 Ma) of U-Pb detrital zircon age results (including four previously published samples). N—number of analyzed zircons. (B) Similar published data from Nepal (first age spectra), southeast Tibet (second age spectra), and Bhutan (remaining spectra). Age spectra marked by asterisks (e.g., "*N = 250") combine results from multiple samples.

TABLE 1. KOLMOGOROV-SMIRNOV STATISTIC APPLIED TO THE PROBABILITY DENSITY FUNCTION OF U-Pb DETRITAL ZIRCON RESULTS

		THS		GHC			LHS			Shillong Group	
		AY 06-29-06 10A	AY 07-01-06 5B	AY 02-13-06 7	AY 02-13-06 8	AY 02-13-06 9B	AY 09-16-03 14A	AY 09-17-03 15	AY 12-31-04 1	AY 02-04-06 12	AY 02-04-06 18
	N	92	83	108	112	108	100	97	95	37	96
AY 07-01-06 5B	*D*	0.31									
	PROB	3E–4									
AY 02-13-06 7	*D*	0.65	0.43								
	PROB	3E–19	2E–8								
AY 02-13-06 8	*D*	0.56	0.32	0.42							
	PROB	1E–14	7E–5	3E–9							
AY 02-13-06 9B	*D*	0.65	0.43	0.17	0.41						
	PROB	2E–19	3E–8	0.068	8E–9						
AY 09-16-03 14A	*D*	0.68	0.51	0.19	0.57	0.34					
	PROB	1E–20	4E–11	0.030	1E–15	5E–6					
AY 09-17-03 15	*D*	0.65	0.44	0.10	0.46	0.24	0.17				
	PROB	3E–18	2E–8	0.631	3E–10	0.005	0.110				
AY 12-31-04 1	*D*	0.83	0.70	0.77	0.92	0.85	0.75	0.75			
	PROB	1E–29	2E–20	3E–27	8E–40	1E–33	3E–25	1E–24			
AY 02-04-06 12	*D*	0.54	0.37	0.30	0.54	0.44	0.23	0.24	0.70		
	PROB	2E–7	0.001	0.010	9E–8	2E–5	0.104	0.080	2E–12		
AY 02-04-06 18	*D*	0.74	0.56	0.31	0.63	0.45	0.17	0.24	0.75	0.28	
	PROB	2E–23	4E–13	1E–4	7E–19	1E–9	0.107	0.006	2E–24	0.024	

Note: N—number of zircon grains analyzed per sample; *D*—maximum vertical separation between the cumulative probability spectra of the indicated samples; PROB—probability of valid null hypothesis (PROB > 0.05 indicates that the distributions being compared are indistinguishable at the 95% confidence level). THS—Tethyan Himalayan Sequence; GHC—Greater Himalayan Crystalline complex; LHS—Lesser Himalayan Sequence.

and LHS samples (Fig. 8; Table 1). Dominated by a single prominent age peak at ca. 1780 Ma, this sample may represent an older stratigraphic unit, perhaps from a nearby pluton with a ca. 1780 Ma crystallization age. The youngest detrital zircon in this sample is a single ca. 1640 Ma grain in the young flank of the ca. 1780 Ma age peak. Depending on the significance assigned to the youngest grain, the interpreted maximum depositional age of this unit is ca. 1640 Ma or ca. 1780 Ma.

U-Pb Ages of Intrusive Rocks

To determine the age of intrusive rocks in the Late Triassic strata, we dated a crosscutting diabase (sample AY 06–29–06 10B in Fig. 5A). We were only able to obtain two zircon separates from the sample, one yielding a ^{207}Pb/^{206}Pb age of 803 ± 73 Ma and the other a ^{238}U/^{206}Pb age of 57 ± 4 Ma (Fig. 9; Table 2; cathodoluminescence images provided in Data Repository Supplementary File 2 [see footnote 1]). We suggest that the older age represents an inherited zircon. A wide range of interpretations could be applied to the younger age: it could represent inherited zircon, the crystallization age of the intrusion, or a mixed age signal affected by Pb-loss/metamorphism.

To evaluate the age of GHC rocks immediately below the South Tibet detachment in southeast Tibet, we dated an augen gneiss unit (sample AY 07–02–06 1 in Fig. 6). We obtained eight analyses from six zircons (Fig. 9; Table 2; cathodoluminescence images provided in Data Repository Supplementary File 2 [see footnote 1]). Five analyses yield UO/U outside the range of calibration, and the analysis below the calibration range has a very large error. Excepting the analysis below the calibration range, the weighted mean ^{207}Pb/^{206}Pb age for the augen gneiss is 485 ± 20 Ma (2σ), which we interpret as the igneous protolith crystallization age.

DISCUSSION

Our field mapping and U-Pb zircon dating across the eastern Himalaya reveal the following: (1) The South Tibet detachment along the Bhutan-China border is a top-to-the-north ductile shear zone; (2) Triassic and Cretaceous THS sedimentary samples show a similar age range of detrital zircons from ca. 200 Ma to ca. 3500 Ma, but Triassic rocks are distinguished by a significant age cluster between ca. 220 and ca. 280 Ma and a well-defined age peak at ca. 570 Ma; (3) a 57 ± 4 Ma date of uncertain significance from a dike crosscutting Late Triassic THS strata; (4) an augen gneiss within the South Tibet detachment shear zone in southeast Tibet has a Cambrian–Ordovician crystallization age; (5) GHC paragneiss and LHS quartzites from the Bhalukpong-Tawang traverse share similar provenance and Late Proterozoic maximum depositional ages; and (6) LHS metagraywacke from the Kimin traverse has a distinct provenance, with a Paleoproterozoic maximum depositional age indicated by a single prominent age peak of ca. 1780 Ma. We discuss broader implications of these findings in the following sections.

Ductile Shear along the South Tibet Detachment at the Bhutan-China Border

Here, we combine the new mapping of the South Tibet detachment along the Bhutan-China border with prior mapping in order to test GHC emplacement models (Fig. 2) across the eastern Himalaya.

Wedge extrusion kinematic models require a north-dipping South Tibet detachment during motion (e.g., Burchfiel and Royden, 1985). However, there is extensive evidence that the South Tibet detachment was subhorizontal during its activity. First, its current orientation is subhorizontal. The main trace is commonly gently north-dipping (e.g., Burchfiel et al., 1992), but its overall orientation is locally warped and nearly flat. Klippen extend up to ~100 km south of the main trace in Bhutan (e.g., Edwards et al., 1996; Grujic et al., 2002; Long and McQuarrie, 2010; Kellett and Grujic, 2012), and high-grade domes up to ~100 km north of the main trace are bounded by the South Tibet detachment (e.g., Chen et al., 1990; Larson et al., 2010b; Wagner et al., 2010; Zhang et al., 2012). Second, there is no thermochronologic offset across the fault. Rather, matching ages are observed or a smooth, slow age increase is observed from the footwall to the hanging wall (e.g., Metcalfe, 1993; Godin et al., 2001; Vannay et al., 2004; Chambers et al., 2009; cf. Coleman and Hodges, 1998; see review by Yin, 2006). This pattern cannot be accomplished if the footwall is exhumed relative to the hanging wall. Third, the cold-over-hot thermal pattern associated with the South

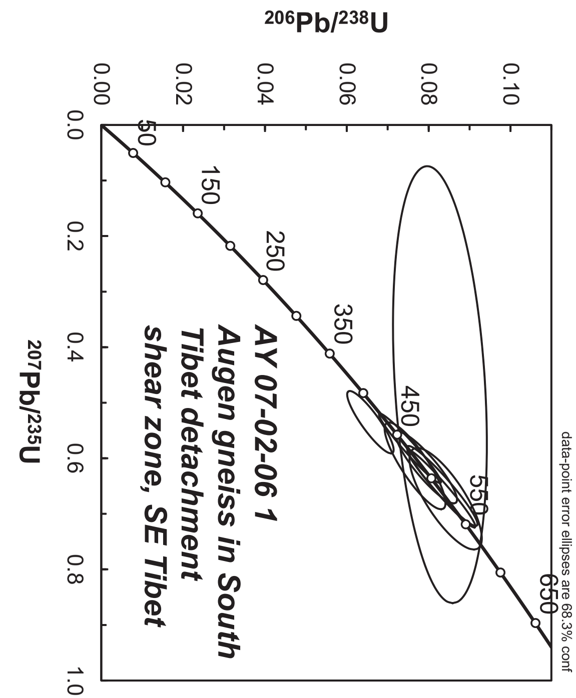

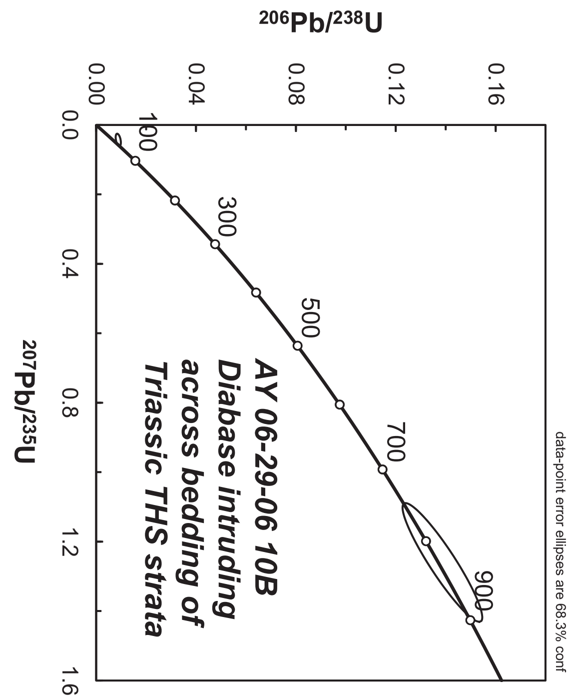

Figure 9. U/Pb concordia diagram showing results of single-spot ion microprobe analyses on zircon from igneous and metaigneous rocks of southeast Tibet. THS—Tethyan Himalayan Sequence.

TABLE 2. ION MICROPROBE U-(Th)-Pb ZIRCON DATA

Spot ID†	Isotopic ratios: $^{206}Pb^*/^{238}U$	±1 s.e.§	$^{207}Pb^*/^{235}U$	±1 s.e.§	$^{207}Pb^*/^{206}Pb^*$	±1 s.e.§	$^{206}Pb^*$ (%)	U (ppm)	UO/U	Th/U	Ages (Ma, ±1 s.e.)§: $^{206}Pb^*/^{238}U$	±		$^{207}Pb^*/^{235}U$	±		$^{207}Pb^*/^{206}Pb^*$	±	
AY 06-29-06 10B								*U-Pb calibration established for UO/U values of:*	9.2–10#										
a, 1	1.39E–01	1.05E–02	1.26E+00	1.13E–01	6.59E–02	2.29E–03	99.0	8.10E+01	9.79	0.640	837.2	±	59.7	827.9	±	50.7	803.0	±	72.7
b, 1	8.86E–03	6.88E–04	4.32E–02	1.19E–02	3.54E–02	8.96E–03	96.0	2.84E+02	9.32	0.536	56.9	±	4.4	42.9	±	11.6		Negative	
AY 07-02-06 1								*U-Pb calibration established for UO/U values of:*	9.2–10#										
a, 1	6.58E–02	3.75E–03	5.35E–01	3.71E–02	5.90E–02	1.90E–03	97.4	8.22E+02	10.71	0.822	410.6	±	22.7	435.1	±	24.5	566.7	±	70.3
a, 2	7.67E–02	4.91E–03	6.14E–01	5.16E–02	5.80E–02	2.56E–03	97.4	3.90E+02	10.28	0.620	476.3	±	29.4	485.8	±	32.5	531.0	±	96.6
b, 1	7.55E–02	5.01E–03	5.82E–01	4.14E–02	5.60E–02	9.71E–04	97.6	1.54E+03	10.09	0.411	468.9	±	30.0	465.8	±	26.6	450.6	±	38.5
b, 2	8.31E–02	5.48E–03	6.55E–01	4.62E–02	5.71E–02	9.51E–04	99.1	1.88E+03	9.95	0.427	514.8	±	32.6	511.4	±	28.4	496.3	±	36.7
c, 1	8.28E–02	7.57E–03	4.68E–01	2.60E–01	4.10E–02	2.20E–02	85.4	6.28E+02	8.48	0.759	512.6	±	45.1	389.4	±	180.0		Negative	
d, 1	8.33E–02	5.68E–03	6.50E–01	4.75E–02	5.66E–02	1.26E–03	97.9	6.65E+02	9.78	0.634	515.9	±	33.8	508.4	±	29.3	474.7	±	49.4
e, 1	8.42E–02	5.83E–03	6.73E–01	6.04E–02	5.80E–02	3.24E–03	97.2	1.46E+02	9.87	1.750	520.9	±	34.7	522.4	±	36.7	529.0	±	122.0
f, 1	7.95E–02	4.90E–03	6.17E–01	4.23E–02	5.63E–02	1.72E–03	96.3	1.20E+03	10.46	0.515	493.2	±	29.3	488.0	±	26.5	464.0	±	67.7

*Radiogenic Pb was corrected for common Pb with composition $^{206}Pb/^{204}Pb = 18.86$, $^{207}Pb/^{204}Pb = 15.62$, $^{208}Pb/^{204}Pb = 38.34$, estimated from model of Stacey and Kramers (1975). Negative apparent ages are due to reverse discordance.

†Spot ID: #, #—zircon name, spot number.

§s.e.—standard error.

Tibet detachment is a gradual transition. Peak metamorphic temperatures decrease monotonically from ~750–650 °C to ~400–350 °C across 100 m scale to kilometer-scale sections across the South Tibet detachment shear zone and immediately adjacent rocks (e.g., Crouzet et al., 2007; Jessup et al., 2008; Cottle et al., 2011). This pattern is essentially constant from the northern Himalayan domes to the southerly klippen (e.g., Lee et al., 2000; Grujic et al., 2002; Kellett and Grujic, 2012). Likewise, microstructural studies show that South Tibetan detachment deformation temperatures are roughly consistent from north to south, showing a sequential evolution from ~700 °C to ~400 °C and continuing deformation down to ~300 °C along the main trace and northern dome exposures (e.g., Jessup et al., 2008; Kellett et al., 2009; Wagner et al., 2010; Law et al., 2011). The cold-over-hot thermal juxtaposition is not accomplished via section-cutting normal faulting, but rather through general shear involving ~50% pure shear (e.g., Jessup et al., 2006; Langille et al., 2010; Cottle et al., 2011). These geometric, thermochronologic, and thermal patterns all support a subhorizontal South Tibet detachment extending ~200 km in the arc-perpendicular direction, ruling out wedge extrusion models.

Channel flow–focused denudation models are largely consistent with a subhorizontal South Tibet detachment. This geometry would be maintained during GHC emplacement, except at the southern terminus during the Miocene, when this part of the structure would have dipped to the north, allowing southward extrusion of the GHC. The recently discovered intersection of the South Tibet detachment and Main Central thrust to the south in the western and central Himalaya, and the corresponding preservation of the leading edge of the GHC preclude southward extrusion there (Yin, 2006; Webb et al., 2007, 2011a, 2011b). Likewise, the Bhutan map pattern shows the southward convergence of the South Tibet detachment and Main Central thrust (e.g., Grujic et al., 2002; Kellett et al., 2009; Chambers et al., 2011; cf. Long and McQuarrie, 2010). These two faults are exposed within 2 km of each other in southern Bhutan. This would be an exceptionally narrow aperture for extrusion, and it is instead interpreted to show that the frontal tip of the GHC has only recently been eroded away in this area (Yin, 2006). Kellett and Grujic (2012) recently introduced a second reason to exclude the channel flow–focused denudation model: the updip (i.e., to the south) progression of fault kinematics along the South Tibet detachment is not consistent with normal faulting. Along the range crest to the north, brittle fabrics are locally associated with this structure (e.g., Law et al., 2011), but in the klippen to the south, the shear zone displays only ductile fabrics.

Remaining models are tectonic wedging and tectonic wedging–low-angle normal fault extrusion (Fig. 2). The latter model is distinguished by late brittle detachment faulting along an upper South Tibet detachment strand that would cut the previously developed, largely ductile lower South Tibet detachment at the range crest. Our new mapping addresses this prediction, because the Bhutan-China border closely coincides with the range crest. The exclusively ductile shear zone we observe is consistent with the South Tibet detachment exposures across the Bhutan klippe, rather than a late brittle detachment cutting that structure. Burchfiel et al. (1992) and Edwards et al. (1996) also mapped along the GHC–THS contact exposed near the Bhutan-China border. They speculated that brittle South Tibet detachment strands occur there, although both groups of authors agree there is no evidence for a brittle detachment along a South Tibet detachment exposure defined by a ductile shear zone occurring ~10 km to the northeast of our new mapping. Edwards et al. (1996) inferred a brittle detachment ~50 km to the west based on a lithologic contact, but only ductile fabrics are reported, and the description of lithologies and metamorphic grade above and below the contact is consistent with the ductile shear zone exposures. Another ~50 km to the west, Burchfiel et al. (1992) inferred a low-angle, north-dipping brittle detachment beneath Quaternary fill (at their Wagye La transect). The inferred detachment separates ductile shear zone rocks from THS and Cenozoic sediments. However, the necessary pre-Quaternary juxtaposition could be readily accomplished along northwest- and northeast-striking steep normal faults. Such normal faults are the dominant structures in the area and are presumably associated with the adjacent Yadong rift (e.g., Taylor et al., 2003). Finally, both author groups show that one steep brittle normal fault (the Zhong Chu fault) locally juxtaposes THS and shear zone rocks. They also noted that it directly juxtaposes Mesozoic THS strata in the footwall against Mesozoic THS strata in the hanging wall, suggesting a modest (<3–4 km) total slip. In short, evidence for a major low-angle normal fault along the range crest north of Bhutan is equivocal at best. We therefore favor the tectonic wedging model for the eastern Himalaya. A medium- to low-temperature thermochronological investigation across the potential upper South Tibet detachment would provide another test of the tectonic wedging–low-angle normal fault extrusion model. As discussed already herein, results from such studies to the west are inconsistent with normal faulting (Yin, 2006).

Origin of Late Triassic THS Strata and Implications for Timing of India-Lhasa Rifting

The dominant range of detrital zircon age spectra for both the Early Cretaceous THS sample and the Late Triassic THS sample, and existing detrital zircon geochronology of Late Triassic THS rocks north of the Lhunze thrust in southeast Tibet by Aikman et al. (2008) and Li et al. (2010) (Fig. 8) extends from ca. 500 Ma to ca. 3000 Ma, with a concentration between ca. 500 Ma and ca. 1000 Ma. This pattern is typical of the THS, GHC, and Lhasa terrane (e.g., DeCelles et al., 2000; Martin et al., 2005; Leier et al., 2007; Gehrels et al., 2011), and therefore suggests Gondwanan provenance for Mesozoic sediments in southeast Tibet. However, the Triassic population is differentiable from the Cretaceous results on the basis of a substantial group of ca. 200–300 Ma zircons in the former, which Hf isotopic signatures indicate come from juvenile crust (Li et al., 2010). As discussed earlier herein, there is no known source for these zircons in northern India, and paleocurrent observations suggest that the sediments are derived from the north (Li et al., 2003a, 2003b, 2004). Three proposed models for the deposition of the Late Triassic rocks, i.e., the rift-fill, Lhasa forearc, and intra-oceanic forearc models, were discussed earlier herein and are shown in Figure 3.

A critical distinction between the three models is that only the rift-fill model involves deposition of the Late Triassic rocks along the northern Indian margin. Therefore, a potentially important geological relationship is the intrusion of the Late Triassic rocks by diabase sills and dikes (e.g., Fig. 7C). These intrusive units may correlate with similar 145–130 Ma intrusions and volcanics associated with Early Cretaceous THS strata across southeast Tibet (Zhu et al., 2005, 2007, 2008; Dunkl et al., 2011). The 145–130 Ma rocks are interpreted to reflect initial magmatism of the Kerguelen plume. Therefore, crosscutting of Late Triassic strata by these igneous rocks would place the Late Triassic strata along the northern Indian margin in the Early Cretaceous. We attempted to test this possibility by dating a sample from a diabase crosscutting Late Triassic strata, but our limited zircon yield (2 grains) afforded only one possible crystallization age date of 57 ± 4 Ma. K-Ar dates of metamorphic muscovite in these rocks are ca. 44 Ma (Dunkl et al., 2011), so the 57 Ma datum may be affected by Pb loss during metamorphism. Nonetheless, the diabase lithology and contact relationships, as well as Early Cretaceous illite growth in surrounding strata (Dunkl et al., 2011), continue to favor correlation of these diabase intrusions with the

Geological Society of America Bulletin, published online on 21 November 2012 as doi:10.1130/B30626.1

145–130 Ma igneous rocks. We therefore favor a rift-fill model. Dai et al. (2008) suggested that a possible source for rift-fill detritus could be an arc developed along the northern Lhasa terrane margin, perhaps as a result of subduction of Mesotethys Ocean lithosphere. The juvenile crustal signature evinced by the Hf isotopic record of the youngest detrital zircons (Li et al., 2010) indicates an arc source, so we include the northern Lhasa arc as a necessary component of the rift-fill model.

Chronostratigraphy of the Eastern Himalaya

The three dated GHC paragneiss samples from the Bhalukpong-Tawang traverse show similar provenance to LHS quartzite arenite samples from the same traverse (Yin et al., 2006), sharing Late Proterozoic maximum depositional ages and, in one case, indistinguishable age spectra at the 95% confidence level based on a Kolmogorov-Smirnov test (Table 1). These GHC and LHS strata appear to be derived from similar sources, and they may occur as a single stratigraphic unit that is duplicated by the Main Central thrust in this region. This interpretation is consistent with an Indian source and depositional environment for both GHC and LHS protoliths.

The LHS sample from the Kimin traverse, some 200 km east of the Bhalukpong-Tawang traverse (sample AY 12–31–04 1 in Fig. 5C), shows a very different age pattern, with a Paleoproterozoic maximum depositional age. This highlights along-strike heterogeneity in LHS stratigraphy. The aforementioned GHC samples show one significant variation: The sample from an intermediate structural horizon has a ca. 0.83 Ga youngest age peak, whereas the upper and lower samples have similar, older youngest age peaks of ca. 0.99 and ca. 1.01 Ga. This could reflect structural duplication of a subunit containing the upper and lower sampled horizons.

Correlations of Eastern Himalayan and NE Indian Cratonal Units

Moderately to weakly defined age peaks at ca. 1110 Ma occur in most of the samples from the THS, GHC, and LHS units of the eastern Himalayan and from the Proterozoic Shillong Group in NE India (Fig. 8). The exceptions are sample AY 12–31–04 1 from the LHS in the Kimin traverse and sample AY 02–04–06 18 from the Shillong Group (Fig. 8). These samples have the youngest age peaks at ca. 1780 Ma and ca. 1190 Ma, respectively, indicating that they may have been deposited prior to 1110 Ma. Granitic gneisses of ca. 1100 Ma may have served as a common source for the 1110 Ma zircon in both the eastern Himalayan and Shillong samples; orthogneiss of this age occurs in the nearby Indian craton (Yin et al., 2010a) and may occur in the Bhutan LHS (Bhargava, 1995). The ca. 1110 Ma signal in Triassic THS rocks may indicate an Indian craton source for these rocks, or detrital input from both India and Lhasa, in contrast to the exclusively northern-source interpretations of Dai et al. (2008) and Li et al. (2010). Alternatively, if the northern-source interpretation is maintained, this signal would suggest similar basement evolution in the Lhasa block and Indian craton (cf. Gehrels et al., 2011).

Zircons with ages of 1600–1750 Ma occur as a major or minor component of all age spectra of the Arunachal samples except sample AY 12–31–04 1 from the Kimin traverse, which was possibly deposited prior to this time period. Although 1600–1750 Ma zircons are a common minor component in age spectra from across the Himalaya (e.g., Gehrels et al., 2003), their major presence in some zircon-age populations may be unique to Arunachal, and may reflect significant along-strike differences in source-to-sink pathways prior to the Cenozoic deformation. Moderately to weakly defined peaks in the relative probability plots may indicate two dominant age groups within the 1600–1750 Ma time window: (1) 1630–1650 Ma (evidenced by age spectra of samples AY 09–16–03 14A, AY 9–17–03 15, AY 02–04–06 12, AY 02–04–06 18, and perhaps by samples AY 07–01–06 5B and AY 02–13–06 7), and (2) ca. 1730 Ma age (evidenced by age spectra of samples AY 02–13–06 7 and AY 02–04–06 12 and perhaps by samples AY 9–17–03 15 and AY 02–04–06 18). The ca. 1730 Ma ages could correlate with ca. 1745 Ma granitic gneisses that occur in both the GHC and LHS of the Arunachal Himalaya (Yin et al., 2010a). The presence of zircon with these ages in the Shillong Group (as in sample AY 02–04–06 12 and possibly sample AY 02–04–06 18) may thus provide another link between the Himalayan units and the Indian craton stratigraphy.

In general, the dominance of Middle Proterozoic detrital zircons common to GHC, Bhalukpong LHS, and Shillong Group samples suggests the possible existence of a regionally correlative Late Proterozoic unit spanning this portion of the northern Indian margin. A summary of the age relationships obtained from this study and those from McQuarrie et al. (2008), Tobgay et al. (2010), Long et al. (2011a), Hughes et al. (2011), and McKenzie et al. (2011) is shown in Figure 10. The Arunachal Lesser Himalayan sedimentary units may correlate with the Jaishidanda Formation and possibly the Baxa Group of Bhutan to the west (Figs. 8B and 10; McQuarrie et al., 2008; Tobgay et al., 2010; Long et al., 2011a). Likewise, the age spectrum of the Kimin LHS sample suggests a possible correlation to the Paleoproterozoic Daling-Shumar Group of the Bhutan Lesser Himalayan Sequence to the west (McQuarrie et al., 2008; Tobgay et al., 2010; Long et al., 2011a). Both of these correlations may extend to include Late Proterozoic and Paleoproterozoic clastic units along the whole length of the Himalaya as suggested by Long et al. (2011a).

Crustal Architecture of NE India in the Early Paleozoic

The eastern Himalayan orogen (east of the Sikkim Himalaya) is unique in that it has a narrow foreland basin along its southern margin (Yin, 2006). As a result, basement rocks of the Indian craton are exposed as close as only 30 km from the Himalayan frontal thrust zone (Gansser, 1983). Recent work in the eastern Himalaya, including Bhutan and Arunachal and the work from Shillong Plateau, allows us to make a preliminary reconstruction of the structural architecture of the NE Indian continental margin prior to the Cenozoic India-Asia collision. As shown in Yin et al. (2010a, 2010b), the Arunachal Himalaya and the NE Indian craton share a common geologic history from Paleoproterozoic to Late Cambrian–Early Ordovician time. Specifically, both areas experienced magmatism at ca. 1.65–1.75 Ga, ca. 1.1 Ga, and 550–460 Ma. In the Shillong region, a deformation event can be bracketed from deformed and undeformed early Paleozoic plutonic rocks at around 520–480 Ma. Although there is no direct evidence in the eastern Himalaya for this early Paleozoic deformation event, the marked change in the Lesser Himalayan stratigraphy across the Arunachal Himalaya between the Bhalukpong-Tawang and Kimin traverses led Yin et al. (2010b) to suggest that the NE-striking Shilling thrust may have extended into the eastern Himalaya, causing juxtaposition of different Proterozoic rocks across its inferred trace.

Based on the existing age data summarized in Figure 11, we suggest that both the eastern Himalaya and NE Indian craton had crystalline basement rocks comprising augen gneisses with ages mostly greater than 1750–1650 Ma. The lower Rupa Group exposed in the Kimin traverse and the lower Shillong Group exposed in NE India may represent the oldest sedimentary cover sequence on top of the basement. This lower sequence may have been locally intruded by the 1.1 Ga plutons (Fig. 11). The majority of the Proterozoic sediments in NE India and the eastern Himalaya appear to have been deposited in the period of 1.1 Ga and 560 Ma, and they

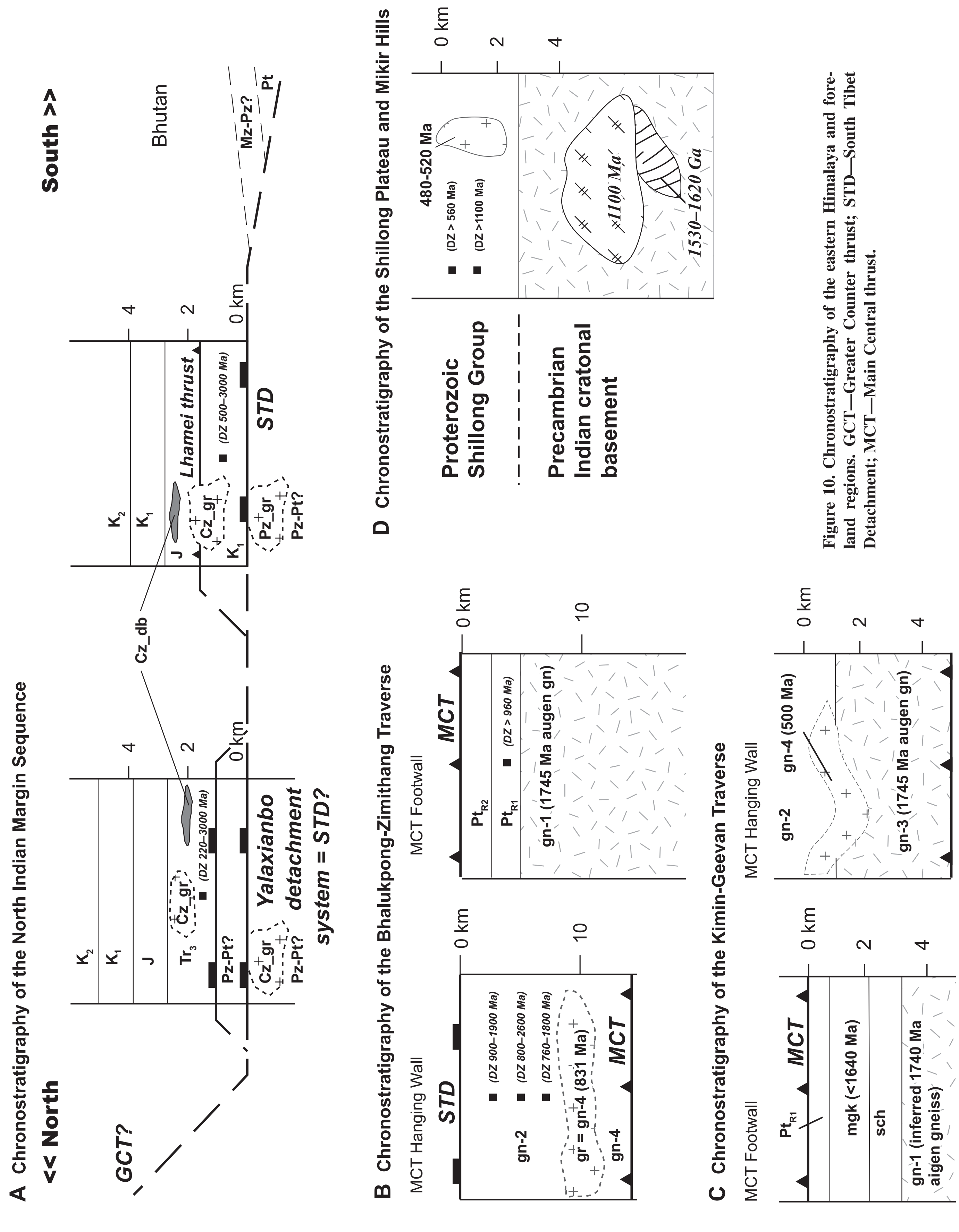

Figure 10. Chronostratigraphy of the eastern Himalaya and foreland regions. GCT—Greater Counter thrust; STD—South Tibet Detachment; MCT—Main Central thrust.

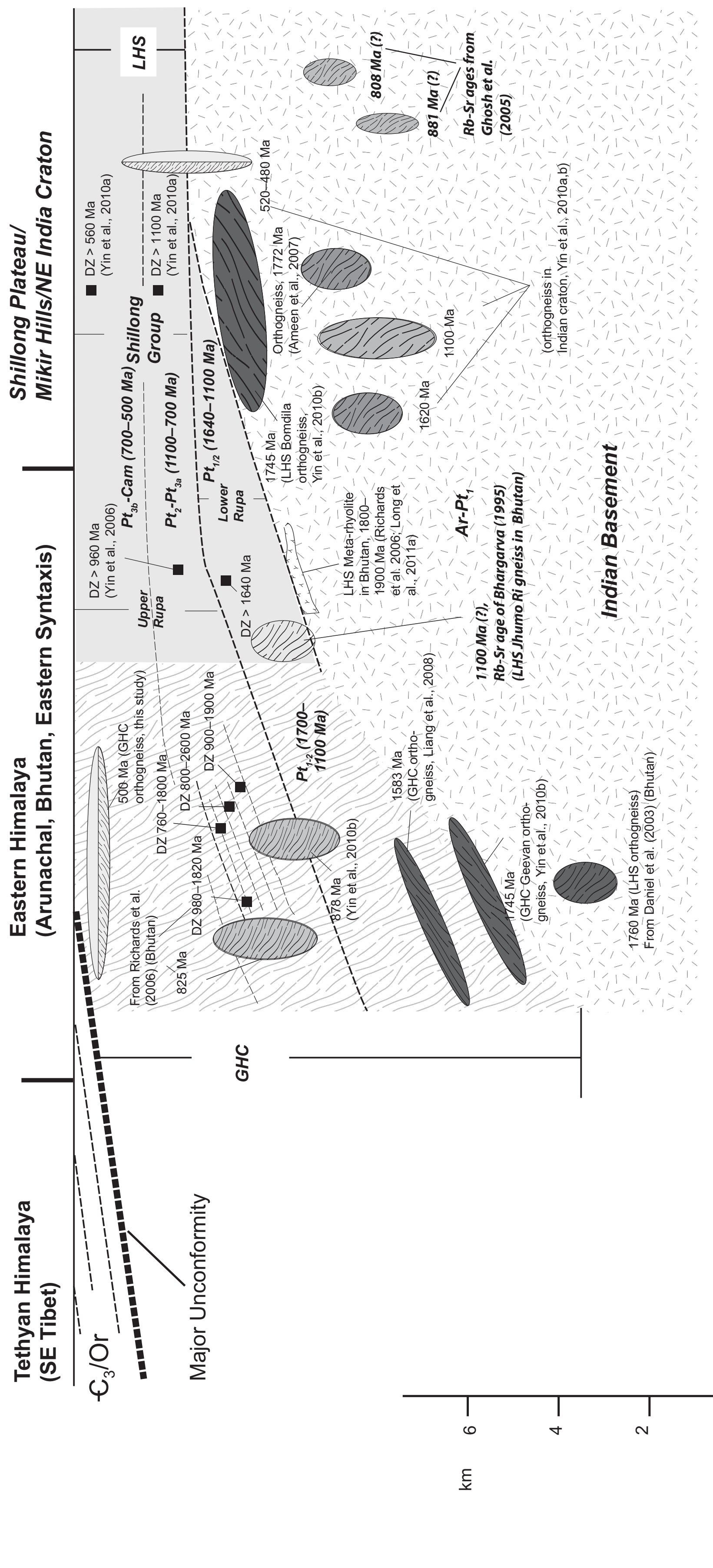

Figure 11. Interpreted crustal architecture of the northeastern Indian craton and eastern Himalaya in Cambrian–Ordovician time. Except those specifically indicated as Rb-Sr whole-rock isochron ages, all of the ages in the diagram were obtained from the U-Pb zircon dating method. See text for detailed discussion. GHC—Greater Himalayan Crystalline complex; LHS—Lesser Himalayan Sequence.

are intruded by plutons with ages mostly in the range of 520–480 Ma. If the youngest zircon ages in the GHC represent their true depositional ages, it appears that the GHC rocks are mostly correlated with the middle section of the cover sequence that was deposited after the deposition of the lower Rupa Group but prior to the massive plutonic intrusion between 520 Ma and 480 Ma in the region (Fig. 11).

Late Triassic–Late Cenozoic Tectonic Evolution of the Eastern Himalaya

We compile our results into a new model for the tectonic evolution of the eastern Himalaya since the Late Triassic, as presented in a series of schematic cross sections (Fig. 12). The first stage depicts the deposition of the Late Triassic THS strata during India-Asia rifting, in accordance with the rift-fill model (Dai et al., 2008). The model is modified to include subduction of the Mesotethys along the northern Lhasa terrane margin, thereby providing a source of 200–300 Ma zircons with juvenile crustal Hf isotopic signatures (cf. Li et al., 2010). Excepting the 200–300 Ma age population, detrital zircon age patterns from the Lhasa terrane are largely similar to age spectra from the northern margin of India (Leier et al., 2007; Gehrels et al., 2011). The interpreted pre-Triassic contiguity of the Lhasa terrane and India is consistent with this observation.

After rifting and drifting, the tectonic evolution followed a Wilson cycle pattern (Wilson, 1966): The ocean basin collapsed via a subduction margin developed along the southern margin of the Lhasa terrane. The second schematic cross section depicts the late phase of ocean basin closure, just prior to the initiation of continent-continent collision of India with the Lhasa terrane at ca. 65–50 Ma (Fig. 12; e.g., Yin and Harrison, 2000; Cai et al., 2011). Dashed lines mark major boundaries that developed in the next time step, i.e., the base of the Himalayan orogenic wedge during early collision and the Gangdese thrust. A southerly pinch-out of Triassic and Jurassic strata is included as a potential explanation for arc-perpendicular changes in South Tibetan detachment hanging-wall stratigraphy, as discussed in the following.

The third schematic diagram depicts the Himalayan orogenic wedge prior to synchronous motion along the Main Central thrust and South Tibetan detachment. The northern portions of the orogenic wedge show internal thickening of units during shortening (e.g., Yin et al., 1999; Antolín et al., 2010, 2011; Dunkl et al., 2011). Cenozoic granite crosscut folds developed during the early thickening (as displayed in the inset), constraining at least some initial

Geological Society of America Bulletin, published online on 21 November 2012 as doi:10.1130/B30626.1

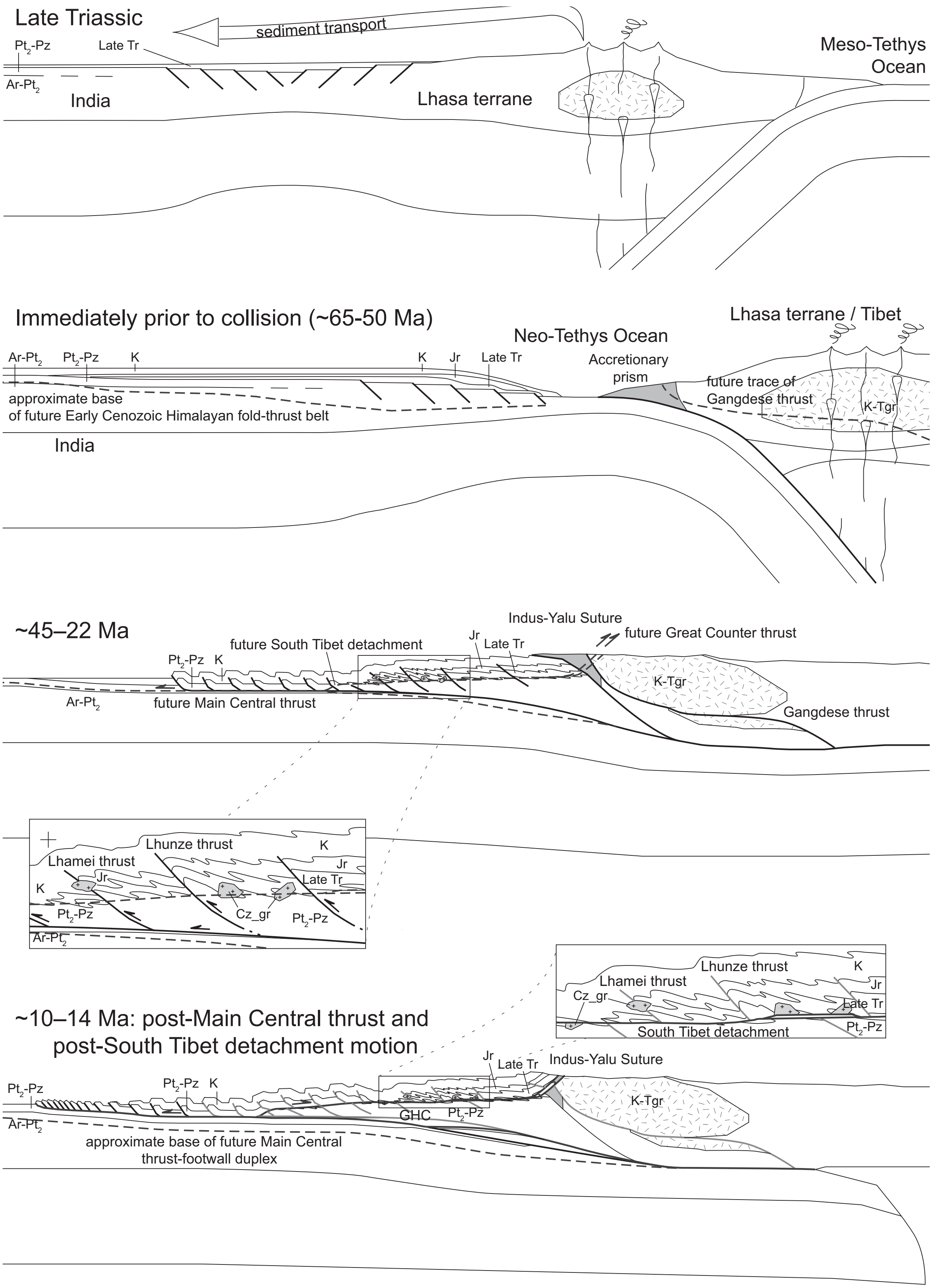

Figure 12. Schematic cross sections showing the Late Triassic–late Cenozoic tectonic evolution of the eastern Himalaya. Detailed description is provided in the text ("Late Triassic–Late Cenozoic Tectonic Evolution of the Eastern Himalaya" section).

shortening to precede ca. 44 Ma (Aikman et al., 2008). Cessation of illite growth at ca. 24–22 Ma is interpreted by Dunkl et al. (2011) to indicate the end of this shortening period within the main Himalayan wedge. Although some thrust propagation across the THS is shown to penetrate into the GHC in this diagram, clearly there are many possible kinematic histories for internal GHC deformation across the time period represented by this diagram. These include GHC growth via channel tunneling (e.g., Beaumont et al., 2001) or underplating (e.g., Corrie and Kohn, 2011). Our data do not shed new light on these processes, but the schematic geometry is compatible with both models. To the north, two concepts are proposed for hinterland deformation between ca. 32 and ca. 25 Ma: Shortening continues, concentrated along the Gangdese thrust (Figs. 4, 5, and 12; Yin et al., 1994, 1999); or regional extension occurs along the Indus-Tsangpo suture in response to rollback of the downgoing Indian plate beneath Tibet (DeCelles et al., 2011; Zhang et al., 2011). Both mechanisms result in uplift of the Gangdese batholith, accomplishing necessary initial conditions for the development of the Great Counter thrust system (which places suture zone and THS rocks atop the Gangdese batholith). Here, we show the Gangdese thrust, which is mapped in the eastern Himalaya (Yin et al., 1999); evidence for extension is currently limited to the western and west-central Himalaya (DeCelles et al., 2011; Zhang et al., 2011). The early Miocene development of the Main Central thrust, South Tibetan detachment, and Great Counter thrust follows this period, so the predeformation traces of these structures are highlighted by dashed lines in the third schematic cross section. A tectonic wedging kinematic model is shown. The South Tibetan detachment trace is interpreted to cut a path that roughly corresponds to the warped base of the Mesozoic strata, which could correspond to a strength discontinuity and may roughly coincide with the brittle-ductile transition (cf. Kellett and Grujic, 2012).

The fourth schematic cross section shows the orogenic wedge after coeval motion along the Main Central thrust and South Tibetan detachment ceased. The path of the predeformation and deformed South Tibetan detachment through the shortened north Indian stratigraphy shows how a pinch-out of Triassic and Jurassic strata could achieve arc-perpendicular changes in South Tibetan detachment hanging-wall stratigraphy. Another end-member solution could be a South Tibetan detachment that cuts across large-scale folds of the THS section. Below the Main Central thrust, initial duplexing of footwall rocks in the hinterland is shown, with a dashed line indicating the approximate base of Main Central thrust footwall duplex development up to the present (e.g., Bollinger et al., 2004; Nàbelek et al., 2009). Continued growth of the Main Central thrust footwall duplex is the most likely cause for warping of the Main Central thrust, South Tibetan detachment, and the rocks in their hanging walls (e.g., Robinson et al., 2003; King et al., 2011).

In the reconstruction, the paths of the Main Central thrust and South Tibetan detachment cutting across stratigraphy satisfy the many new observations presented here and by Yin et al. (2010a, 2010b) indicating that the LHS, GHC, THS, and foreland basement of the eastern Himalaya contain at least some matching stratigraphic sequences. This demonstrates the general viability of models involving thrusting of the north Indian margin (e.g., Heim and Gansser, 1939) for construction of the Himalayan orogen, even if small portions of the margin sequences are sourced from elsewhere (Dai et al., 2008; Li et al., 2010).

CONCLUSIONS

This work offers new constraints on the provenance of rocks across the eastern Himalaya and the development of the Himalayan orogen. U-Pb geochronology of igneous and detrital zircons establishes the chronostratigraphy and informs models for the Cambrian–Ordovician northeastern Indian margin and the tectonic evolution of this region since it rifted from the Lhasa terrane. Detrital zircons in Late Triassic and Early Cretaceous THS rocks share a similar age range of ca. 3500 to ca. 200 Ma, but Late Triassic rocks are distinguished by a well-defined age peak at ca. 570 Ma and a significant age cluster between ca. 280 and ca. 220 Ma. The young age cluster represents material that was (1) derived from an arc developed along the northern margin of the Lhasa terrane and (2) deposited on the northern margin of India during India-Lhasa rifting. GHC paragneiss from the Bhalukpong-Tawang traverse shares Late Proterozoic maximum depositional ages and general age spectra characteristics with LHS quartzites exposed along this same traverse. However, LHS metagraywacke from the Kimin traverse has a Paleoproterozoic maximum depositional age, indicated by a single prominent age peak of ca. 1780 Ma, indicating along-strike heterogeneity in LHS chronostratigraphy. Nonetheless, the Late Proterozoic rocks in the LHS and GHC along the Bhalukpong traverse can be correlated to each other, and to previously analyzed THS rocks to the west and crystalline rocks of the Indian craton. New field mapping of the South Tibetan detachment along the Bhutan-China border is integrated with existing knowledge to test models of GHC emplacement. Only tectonic models featuring early-middle Miocene southward emplacement of the GHC between two subhorizontal shear zones that intersect to the south—i.e., tectonic wedging models—can satisfy current constraints. We synthesize our results in a reconstruction showing Late Triassic India-Lhasa rifting and Cenozoic eastern Himalayan construction via in situ thrusting of basement and cover sequences along the north Indian margin.

ACKNOWLEDGMENTS

Kyle Larson, an anonymous reviewer, and editors Christian Koeberl and Stefano Mazzoli provided highly constructive feedback. Discussions with Aaron Martin and Dian He improved our ideas. We thank George Gehrels and Victor Valencia for analytical support and geological discussions at the Arizona LaserChron Center, and Marty Grove and Axel Schmitt for similar contributions at the CAMECA IMS 1270 ion microprobe facility at the University of California–Los Angeles. Both facilities are supported by the Instrumentation and Facilities Program, Division of Earth Sciences, National Science Foundation (NSF). This research was supported by NSF Tectonics grants and a start-up grant from Louisiana State University.

REFERENCES CITED

Aikman, A.B., 2007, Tectonics of the Eastern Tethyan Himalaya [Ph.D. thesis]: The Australia National University.

Aikman, A.B., Harrison, T.M., and Lin, D., 2008, Evidence for early (>44 Ma) Himalayan crustal thickening, Tethyan Himalaya, southeastern Tibet: Earth and Planetary Science Letters, v. 274, p. 14–23, doi:10.1016/j.epsl.2008.06.038.

Ameen, S.M.M., Wilde, S.A., Kabir, Z., Akon, E., Chowdhury, K.R., and Khan, S.H., 2007, Paleoproterozoic granitoids in the basement of Bangladesh: A piece of the Indian shield or an exotic fragment of the Gondwana jigsaw?: Gondwana Research, v. 12, p. 380–387, doi:10.1016/j.gr.2007.02.001.

Antolín, B., Appel, E., Gloaguen, R., Dunkl, I., Ding, L., Montomoli, C., Liebke, U., and Xu, Q., 2010, Paleomagnetic evidence for clockwise rotation and tilting in eastern Tethyan Himalaya (SE Tibet): Implications for the Miocene tectonic evolution of the NE Himalaya: Tectonophysics, v. 493, p. 172–186, doi:10.1016/j.tecto.2010.07.015.

Antolín, B., Appel, E., Montomoli, C., Dunkl, I., Ding, L., Gloaguen, R., and El Bay, R., 2011, Kinematic evolution of the eastern Tethyan Himalaya: Constraints from magnetic fabric and structural properties of the Triassic flysch in SE Tibet: Geological Society of London Special Publication 349, p. 99–121, doi:10.1144/SP349.6.

Argand, E., 1924, Extrait du Compte-rendu du XIIIe Congres geologique international 1922 (Liege): v. 1, p. 171–372.

Beaumont, C., Jamieson, R.A., Nguyen, M.H., and Lee, B., 2001, Himalayan tectonics explained by extrusion of a low-viscosity crustal channel coupled to focused surface denudation: Nature, v. 414, p. 738–742, doi:10.1038/414738a.

Beaumont, C., Jamieson, R.A., Nguyen, M.H., and Medvedev, S., 2004, Crustal channel flows: 1. Numerical models with applications to the tectonics of the Himalayan-Tibetan orogen: Journal of Geophysical Research, v. 109, B06406, doi:10.1029/2003JB002809.

Beyssac, O., Bollinger, L., Avouac, J.P., and Goffe, B., 2004, Thermal metamorphism in the Lesser Himalaya of Nepal determined from Raman spectroscopy of carbonaceous material: Earth and Planetary Science Letters, v. 225, p. 233–241, doi:10.1016/j.epsl.2004.05.023.

Bhargava, O.N., 1995, The Bhutan Himalaya: A Geological Account: Geological Survey of India Special Publication 39, 244 p.

Bilham, R., and England, P., 2001, Plateau 'pop-up' in the Great 1897 Assam earthquake: Nature, v. 410, p. 806–809, doi:10.1038/35071057.

Biswas, S., and Grasemann, B., 2005, Quantitative morphotectonics of the southern Shillong Plateau (Bangladesh/India): Australian Journal of Earth Sciences, v. 97, p. 82–103.

Biswas, S., Coutand, I., Grujic, D., Hager, C., Stockli, D., and Grasemann, B., 2007, Exhumation and uplift of the Shillong Plateau and its influence on the eastern Himalayas: New constraints from apatite and zircon (U-Th-[Sm])/He and apatite fission track analyses: Tectonics, v. 26, TC6013, doi:10.1029/2007TC002125.

Bollinger, L., Avouac, J.P., Beyssac, O., Catlos, E.J., Harrison, T.M., Grove, M., Goffé, B., and Sapkota, S., 2004, Thermal structure and exhumation history of the Lesser Himalaya: Tectonics, TC5015, v. 23, doi:10.1029/2003TC001564.

Burchfiel, B.C., and Royden, L.H., 1985, North-south extension within the convergent Himalayan region: Geology, v. 13, p. 679–682, doi:10.1130/0091-7613(1985)13<679:NEWTCH>2.0.CO;2.

Burchfiel, B.C., Zhiliang, C., Hodges, K.V., Yuping, L., Royden, L.H., Changrong, D., and Jiene, X., 1992, The South Tibetan detachment system, Himalayan orogen: Extension contemporaneous with and parallel to shortening in a collisional mountain belt: Geological Society of America Special Paper 269, 41 p.

Burg, J.P., Brunel, M., Gapais, D., Chen, G.M., and Liu, G.H., 1984, Deformation of leucogranites of the crystalline Main Central Sheet in southern Tibet (China): Journal of Structural Geology, v. 6, no. 5, p. 535–542, doi:10.1016/0191-8141(84)90063-4.

Caby, R., Pecher, A., and LeFort, P., 1983, Le grande chevauchement central Himalayen: Nouvelles donnees sur le metamorphisme inverse a la base de la Dalle du Tibet: Revue de Geographie Physiqueau et Geologie Dynamique, v. 24, p. 89–100.

Cai, F., Ding, L., and Yue, Y., 2011, Provenance analysis of Upper Cretaceous strata in the Tethys Himalaya, southern Tibet: Implications for timing of India–Asia collision: Earth and Planetary Science Letters, v. 305, p. 195–206, doi:10.1016/j.epsl.2011.02.055.

Carosi, R., Lombardo, B., Molli, G., Musumeci, G., and Pertusati, P.C., 1998, The South Tibetan detachment system in the Rongbuk valley, Everest region: Deformation features and geological implications: Journal of Asian Earth Sciences, v. 16, p. 299–311, doi:10.1016/S0743-9547(98)00014-2.

Carosi, R., Montomoli, C., Rubatto, D., and Visona, D., 2006, Normal-sense shear zones in the fore of the Higher Himalayan Crystallines (Bhutan Himalaya): Evidence for extrusion?, *in* Law, R.D., Searle, M.P., and Godin, L., eds., Channel Flow, Ductile Extrusion and Exhumation in Continental Collision Zones: Geological Society of London Special Publication 268, p. 425–444.

Célérier, J., Harrison, T.M., Webb, A.A.G., and Yin, A., 2009a, The Kumaun and Garwhal Lesser Himalaya, India: Part 1. Structure and stratigraphy: Geological Society of America Bulletin, v. 121, p. 1262–1280, doi:10.1130/B26344.1.

Célérier, J., Harrison, T.M., Beyssac, O., Herman, F., Dunlap, W.J., and Webb, A.A.G., 2009b, The Kumaun and Garwhal Lesser Himalaya, India: Part 2. Thermal and deformation histories: Geological Society of America Bulletin, v. 121, p. 1281–1297, doi:10.1130/B26343.1.

Chambers, J., Caddick, M., Argles, T., Horstwood, M., Sherlock, S., Harris, N., Parrish, R., and Ahmad, T., 2009, Empirical constraints on extrusion mechanisms from the upper margin of an exhumed high-grade orogenic core, Sutlej valley, NW India: Tectonophysics, v. 477, p. 77–92, doi:10.1016/j.tecto.2008.10.013.

Chambers, J., Parrish, R., Argles, T., Harris, N., and Horstwood, M., 2011, A short-duration pulse of ductile normal shear on the outer South Tibetan detachment in Bhutan: Alternating channel flow and critical taper mechanics of the eastern Himalaya: Tectonics, v. 30, TC2005, doi:10.1029/2010TC002784.

Chen, Z., Liu, Y., Hodges, K.V., Burchfiel, B.C., Royden, L.H., and Deng, C., 1990, The Kangmar dome—A metamorphic core complex in southern Xizang (Tibet): Science, v. 250, p. 1552–1556, doi:10.1126/science.250.4987.1552.

Clift, P.D., Hodges, K., Heslop, D., Hannigan, R., Hoang, L.V., and Calves, G., 2008, Correlation of Himalayan exhumation rates and Asian monsoon intensity: Nature Geoscience, v. 1, p. 875–880, doi:10.1038/ngeo351.

Coleman, M.E., and Hodges, K.V., 1998, Contrasting Oligocene and Miocene thermal histories from the hanging wall and footwall of the South Tibetan detachment in central Himalaya from Ar-40/Ar-39 thermochronology, Marsyandi Valley, central Nepal: Tectonics, v. 17, p. 726–740, doi:10.1029/98TC02777.

Corfield, R.L., and Searle, M.P., 2000, Crustal shortening across the north Indian continental margin, Ladakh, India, *in* Khan, M.A., Treloar, P.J., Searle, M.P., and Jan, M.Q., eds., Tectonics of the Nanga Parbat Syntaxis and the Western Himalaya: Geological Society of London Special Publication 170, p. 395–410.

Corrie, S.L., and Kohn, M.J., 2011, Metamorphic history of the central Himalaya, Annapurna region, Nepal, and implications for tectonic models: Geological Society of America Bulletin, v. 123, p. 1863–1879, doi:10.1130/B30376.1.

Corrie, S.L., Kohn, M.J., and Vervoort, J.D., 2010, Young eclogite from the Greater Himalayan sequence, eastern Nepal; high-precision geochronology and tectonic implications: Earth and Planetary Science Letters, v. 289, p. 406–416, doi:10.1016/j.epsl.2009.11.029.

Cottle, J.M., Waters, D.J., Riley, D., Beyssac, O., and Jessup, M.J., 2011, Metamorphic history of the South Tibetan detachment system, Mt. Everest region, revealed by RSCM thermometry and phase equilibria modeling: Journal of Metamorphic Geology, v. 29, p. 561–582, doi:10.1111/j.1525-1314.2011.00930.x.

Crawford, A.R., 1969, India, Ceylon and Pakistan: New age data and comparison with Australia: Nature, v. 223, p. 380–384, doi:10.1038/223380a0.

Crouzet, C., Dunkl, I., Paudel, L., Arkai, P., Rainer, T.M., Balogh, K., and Appel, E., 2007, Temperature and age constraints on the metamorphism of the Tethyan Himalaya in central Nepal: A multidisciplinary approach: Journal of Asian Earth Sciences, v. 30, p. 113–130, doi:10.1016/j.jseaes.2006.07.014.

Dahlen, F.A., 1990, Critical taper model of fold-and-thrust belts and accretionary wedges: Annual Review of Earth and Planetary Sciences, v. 18, p. 55–99, doi:10.1146/annurev.ea.18.050190.000415.

Dai, J.G., Yin, A., Liu, W.C., and Wang, C.S., 2008, Nd isotopic compositions of the Tethyan Himalayan Sequence in southeastern Tibet: Science in China, ser. D, Earth Science, v. 51, p. 1306–1316.

Daniel, C.G., Hollister, L.S., Parrish, R.R., and Grujic, D., 2003, Exhumation of the Main Central thrust from lower crustal depths, eastern Bhutan Himalaya: Journal of Metamorphic Geology, v. 21, p. 317–334, doi:10.1046/j.1525-1314.2003.00445.x.

Das Gupta, A.B., and Biswas, A.K., 2000, Geology of Assam: Bangalore, Geological Society of India, 169 p.

Davis, D., Suppe, J., and Dahlen, F.A., 1983, Mechanics of fold-and-thrust belts and accretionary wedges: Journal of Geophysical Research, v. 88, no. B2, p. 1153–1172, doi:10.1029/JB088iB02p01153.

DeCelles, P.G., Gehrels, G.E., Quade, J., Ojha, T.P., Kapp, P.A., and Upreti, B.N., 1998, Neogene foreland basin deposits, erosional unroofing, and the kinematic history of the Himalayan fold-thrust belt, western Nepal: Geological Society of America Bulletin, v. 110, p. 2–21, doi:10.1130/0016-7606(1998)110<0002:NFBDEU>2.3.CO;2.

DeCelles, P.G., Gehrels, G.E., Quade, J., LaReau, B., and Spurlin, M., 2000, Tectonic implications of U-Pb zircon ages of the Himalayan orogenic belt in Nepal: Science, v. 288, p. 497–499, doi:10.1126/science.288.5465.497.

DeCelles, P.G., Robinson, D.M., Quade, J., Ojha, T.P., Garzione, C.N., Copeland, P., and Upreti, B.N., 2001, Stratigraphy, structure, and tectonic evolution of the Himalayan fold-thrust belt in western Nepal: Tectonics, v. 20, p. 487–509, doi:10.1029/2000TC001226.

DeCelles, P.G., Kapp, P., Quade, J., and Gehrels, G.E., 2011, Oligocene-Miocene Kailas Basin, southwestern Tibet: Record of postcollisional upper-plate extension in the Indus-Yarlung suture zone: Geological Society of America Bulletin, v. 123, p. 1337–1362, doi:10.1130/B30258.1.

Dewey, J.F., and Bird, J.M., 1970, Mountain belts and new global tectonics: Journal of Geophysical Research, v. 75, p. 2625–2647, doi:10.1029/JB075i014p02625.

Dikshitulu, G.R., Pandey, B.K., Krishna, V., and Dhana, R., 1995, Rb/Sr systematics of granitoids of the Central Gneissic Complex, Arunachal Himalaya: Implications on tectonics, stratigraphy, and source: Journal of the Geological Society of India, v. 45, p. 51–56.

Dong, X., Zhang, Z., Liu, F., Wang, W., Yu, F., and Shen, K., 2011, Zircon U-Pb geochronology of the Nyainqentanglha Group from the Lhasa terrane: New constraints on the Triassic orogeny of the south Tibet: Journal of Asian Earth Sciences, v. 42, p. 732–739.

Drukpa, D., Velasco, A.A., and Doser, D.I., 2006, Seismicity in the Kingdom of Bhutan (1937–2003): Evidence for crustal transcurrent deformation: Journal of Geophysical Research, v. 111, B06301, doi:10.1029/2004JB003087.

Dunkl, I., Antolín, B., Wemmer, K., Rantitsch, G., Kienast, M., Montomoli, C., Ding, L., Carosi, R., Appel, E., El Bay, R., Xu, Q., and von Eynatten, H., 2011, Metamorphic evolution of the Tethyan Himalayan flysch in SE Tibet, *in* Gloaguen, R., and Ratschbacher, L., eds., Growth and Collapse of the Tibetan Plateau: Geological Society of London Special Publication 353, p. 45–69.

Edwards, M.A., Kidd, W.S.F., Li, J., Yue, Y., and Clark, M., 1996, Multi-stage development of the Southern Tibet detachment system near Khula Kangri: New data from Gonto La: Tectonophysics, v. 260, p. 1–19, doi:10.1016/0040-1951(96)00073-X.

Fletcher, J.M., Grove, M., Kimbrough, D., Lovera, O., and Gehrels, G., 2007, Ridge-trench interactions and the Neogene tectonic evolution of the Magdalena shelf and southern Gulf of California: Insights from detrital zircon U-Pb ages from the Magdalena fan and adjacent areas: Geological Society of America Bulletin, v. 119, p. 1313–1336, doi:10.1130/B26067.1.

Frank, W., Grasemann, B., Guntli, P., and Miller, C., 1995, Geological Map of the Kishtwar-Chamba-Kulu Region (NW Himalayas, India): Jahrbuch der Geologischen Bundesanstalt, v. 138, p. 299–308.

Gaetani, M., and Garzanti, E., 1991, Multicyclic history of the northern India continental margin (northwestern Himalaya): The American Association of Petroleum Geologists Bulletin, v. 75, p. 1427–1446.

Gansser, A., 1983, Geology of the Bhutan Himalaya: Boston, Birkhäuser Verlag, 181 p.

Gehrels, G.E., DeCelles, P.G., Martin, A., Ojha, T.P., Pinhassi, G., and Upreti, B.N., 2003, Initiation of the Himalayan orogen as an early Paleozoic thin-skinned thrust belt: GSA Today, v. 13, no. 9, p. 4–9, doi:10.1130/1052-5173(2003)13<4:IOTHOA>2.0.CO;2.

Gehrels, G.E., DeCelles, P.G., Ojha, T.P., and Upreti, B.N., 2006, Geologic and U-Th-Pb geochronologic evidence for early Paleozoic tectonism in the Kathmandu thrust sheet, central Nepal Himalaya: Geological Society of America Bulletin, v. 118, p. 185–198, doi:10.1130/B25753.1.

Gehrels, G., Kapp, P., DeCelles, P., Pullen, A., Blakey, R., Weislogel, A., Ding, L., Guynn, J., Martin, A., McQuarrie, N., and Yin, A., 2011, Detrital zircon geochronology of pre-Tertiary strata in the Tibetan-Himalayan orogeny: Tectonics, v. 30, TC5016, doi:10.1029/2011TC002868.

Ghosh, S., Charkraborty, S., Bhalla, J.K., Paul, D.K., Sarkar, A., Bishui, P.K., and Gupta, S.N., 1991, Geochronology and geochemistry of granite plutons from east Khasi Hills, Meghalaya: Journal of the Geological Society of India, v. 37, p. 331–342.

Ghosh, S., Charkraborty, S., Paul, D.K., Bhalla, J.K., Bishui, P.K., and Gupta, S.N., 1994, New Rb-Sr isotopic ages and geochemistry of granitoids from Meghalaya and their significance in Middle and Late Proterozoic crustal evolution: Indian Minerals, v. 48, p. 33–44.

Ghosh, S., Fallick, A.E., Paul, D.K., and Potts, P.J., 2005, Geochemistry and origin of Neoproterozoic granitoids of Meghalaya, northeast India: Implications for linkage with amalgamation of Gondwana supercontinent: Gondwana Research, v. 8, p. 421–432, doi:10.1016/S1342–937X(05)71144–8.

Godin, L., Parrish, R., Brown, R.L., and Hodges, K.V., 2001, Crustal thickening leading to exhumation of the Himalayan metamorphic core of central Nepal: Insight from U-Pb geochronology and $^{40}Ar/^{39}Ar$ thermochronology: Tectonics, v. 20, p. 729–747, doi:10.1029/2000TC001204.

Godin, L., Grujic, D., Law, R.D., and Searle, M.P., 2006, Channel flow, ductile extrusion and exhumation in continental collision zones: An introduction, *in* Law, R.D., Searle, M.P., and Godin, L., eds., Channel Flow, Ductile Extrusion and Exhumation in Continental Collision Zones: Geological Society of London Special Publication 268, p. 1–23, doi:10.1144/GSL.SP.2006.268.01.01.

Greenwood, L.V., Parrish, R.R., Argles, T.W., Warren, C., and Harris, N.B., 2011, Resolving conflicting models for the tectonic assembly of the eastern Himalaya: Journal of Himalayan Earth Sciences, v. 44 (26th Himalaya-Karakorum-Tibet Workshop), p. 20–21.

Grujic, D., Hollister, L.S., and Parrish, R.R., 2002, Himalayan metamorphic sequence as an orogenic channel: Insight from Bhutan: Earth and Planetary Science Letters, v. 198, no. 1–2, p. 177–191, doi:10.1016/S0012-821X(02)00482-X.

Grujic, D., Coutland, I., Bookhagen, B., Bonnet, S., Blythe, A., and Duncan, C., 2006, Climatic forcing of erosion, landscape, and tectonics in the Bhutan Himalayas: Geology, v. 34, p. 801–804, doi:10.1130/G22648.1.

Grujic, D., Warren, C.J., and Wooden, J.L., 2011, Rapid synconvergent exhumation of Miocene-aged lower orogenic crust in the eastern Himalaya: Lithosphere, v. 3, no. 5, p. 346–366, doi:10.1130/L154.1.

Gupta, R.P., and Sen, A.K., 1988, Imprints of Ninety-East Ridge in the Shillong Plateau, Indian Shield: Tectonophysics, v. 154, p. 335–341, doi:10.1016/0040-1951(88)90111-4.

Harrison, T.M., Yin, A., Grove, M., Lovera, O.M., Ryerson, F.J., and Zhou, X.H., 2000, The Zedong window: A record of superposed Tertiary convergence in southeastern Tibet: Journal of Geophysical Research, v. 105, p. 19,211–19,230, doi:10.1029/2000JB900078.

Heim, A., and Gansser, A., 1939, Central Himalaya Geological Observations of the Swiss Expedition 1936: Zurich, Gebrüder Fretz, 246 p.

Herman, F., Copeland, P., Avouac, J.P., Bollinger, L., Maheo, G., Le Fort, P., Rai, S., Foster, D., Pecher, A., Stuwe, K., and Henry, P., 2010, Exhumation, crustal deformation, and thermal structure of the Nepal Himalaya derived from the inversion of thermochronological and thermobarometric data and modeling of the topography: Journal of Geophysical Research, v. 115, B06407, doi:10.1029/2008JB006126.

Hodges, K.V., Parrish, R.R., and Searle, M.P., 1996, Tectonic evolution of the central Annapurna Range, Nepalese Himalayas: Tectonics, v. 15, p. 1264–1291, doi:10.1029/96TC01791.

Hodges, K.V., Hurtado, J.M., and Whipple, K.X., 2001, Southward extrusion of Tibetan crust and its effect on Himalayan tectonics: Tectonics, v. 20, p. 799–809, doi:10.1029/2001TC001281.

Hollister, L.S., and Grujic, D., 2006, Pulse channel flow in Bhutan, *in* Law, R.D., Searle, M.P., and Godin, L., eds., Channel Flow, Ductile Extrusion and Exhumation in Continental Collision Zones: Geological Society of London Special Publication 268, p. 415–423.

Hughes, N.C., Peng, S., Bhargava, O.N., Ahluwalia, A.D., Walia, S., Myrow, P.M., and Parcha, S.K., 2005, Cambrian biostratigraphy of the Tal Group, Lesser Himalaya, India, and early Tsanglangpuan (late Early Cambrian) trilobites from the Nigali Dhar syncline: Geological Magazine, v. 142, p. 57–80, doi:10.1017/S0016756804000366.

Hughes, N.C., Myrow, P.M., McKenzie, N.R., Harper, D.A.T., Bhargava, O.N., Tangri, S.K., Ghalley, K.S., and Fanning, C.M., 2011, Cambrian rocks and faunas of the Wachi La, Black Mountains, Bhutan: Geological Magazine, v. 148, p. 351–379, doi:10.1017/S0016756810000750.

Jangpangi, B.S., 1974, Stratigraphy and tectonics of parts of eastern Bhutan: Himalayan Geology, v. 4, p. 117–136.

Jessup, M.J., Law, R.D., Searle, M.P., and Hubbard, M.S., 2006, Structural evolution and vorticity of flow during extrusion and exhumation of the Greater Himalayan Slab, Mount Everest Massif, Tibet/Nepal: Implications for orogen-scale flow partitioning, *in* Law, R.D., Searle, M.P., and Godin, L., eds., Channel Flow, Ductile Extrusion and Exhumation in Continental Collision Zones: Geological Society of London Special Publication 268, p. 379–414.

Jessup, M.J., Cottle, J.M., Searle, M.P., Law, R.D., Tracy, R.J., Newell, D.L., and Waters, D.J., 2008, *P-T-t-D* paths of the Everest Series schist, Nepal: Journal of Metamorphic Geology, v. 26, p. 717–739, doi:10.1111/j.1525-1314.2008.00784.x.

Kapp, J.L.D., Harrison, T.M., Kapp, P., Grove, M., Lovera, O.M., and Lin, D., 2005, Nyainqentanglha Shan: A window into the tectonic, thermal, and geochemical evolution of the Lhasa block, southern Tibet: Journal of Geophysical Research–Solid Earth, v. 110, B08413, doi:10.1029/2004JB003330.

Kellett, D.A., and Godin, L., 2009, Pre-Miocene deformation of the Himalayan superstructure, Hidden valley, central Nepal: Journal of the Geological Society of London, v. 166, p. 261–275, doi:10.1144/0016-76492008-097.

Kellett, D.A., and Grujic, D., 2012, New insight into the South Tibetan detachment system: Not a single progressive deformation: Tectonics, v. 31, TC2007, doi:10.1029/2011TC002957.

Kellett, D.A., Grujic, D., and Erdmann, S., 2009, Miocene structural reorganization of the South Tibetan detachment, eastern Himalaya: Implications for continental collision: Lithosphere, v. 1, p. 259–281, doi:10.1130/L56.1.

Kellett, D.A., Grujic, D., Warren, C., Cottle, J., Jamieson, R., and Tenzin, T., 2010, Metamorphic history of a syn-convergent orogen-parallel detachment: The South Tibetan detachment system, Bhutan Himalaya: Journal of Metamorphic Geology, v. 28, p. 785–808, doi:10.1111/j.1525-1314.2010.00893.x.

King, J., Harris, N., Argles, T., Parrish, R., and Zhang, H., 2011, Contribution of crustal anatexis to the tectonic evolution of Indian crust beneath southern Tibet: Geological Society of America Bulletin, v. 123, no. 1–2, p. 218–239, doi:10.1130/B30085.1.

Kohn, M.J., 2008, *P-T-t* data from central Nepal support critical taper and repudiate large-scale channel flow of the Greater Himalayan Sequence: Geological Society of America Bulletin, v. 120, p. 259–273, doi:10.1130/B26252.1.

Kumar, G., 1997, Geology of Arunachal Pradesh: Bangalore, Geological Society of India, 217 p.

Langille, J., Lee, J., Hacker, B., and Seward, G., 2010, Middle crustal ductile deformation patterns in southern Tibet: Insights from vorticity studies in Mabja Dome: Journal of Structural Geology, v. 32, p. 70–85, doi:10.1016/j.jsg.2009.08.009.

Larson, K.P., and Godin, L., 2009, Kinematics of the Himalayan metamorphic slab, Dhaulagiri Himal: Implications for the structural framework of the central Nepalese Himalaya: Journal of the Geological Society of London, v. 166, p. 25–43, doi:10.1144/0016-76492007-180.

Larson, K.P., Godin, L., and Price, R.A., 2010a, Relationships between displacement and distortion in orogens: Linking the Himalayan foreland and hinterland in central Nepal: Geological Society of America Bulletin, v. 122, p. 1116–1134, doi:10.1130/B30073.1.

Larson, K.P., Godin, L., Davis, W.J., and Davis, D.W., 2010b, Out-of-sequence deformation and expansion of the Himalayan orogenic wedge: Insight from the Changgo culmination, south central Tibet: Tectonics, v. 29, TC4013, doi:10.1029/2008TC002393.

Law, R.D., Jessup, M.J., Searle, M.P., Francsis, M.K., Waters, D.J., and Cottle, J.M., 2011, Telescoping of isotherms beneath the South Tibetan detachment system, Mount Everest Massif: Journal of Structural Geology, v. 33, p. 1569–1594, doi:10.1016/j.jsg.2011.09.004.

Lee, J., Hacker, B.R., Dinklage, W.S., Wang, Y., Gans, P., Calvert, A., Wan, J.L., Chen, W.J., Blythe, A.E., and McClelland, W., 2000, Evolution of the Kangmar Dome, southern Tibet: structural, petrologic, and thermochronologic constraints: Tectonics, v. 19, p. 872–895.

Le Fort, P., 1975, Himalaya: The collided range. Present knowledge of the continental arc: American Journal of Science, v. 275A, p. 1–44.

Leier, A.L., Kapp, P., Gehrels, G.E., and DeCelles, P.G., 2007, Detrital zircon geochronology of Carboniferous-Cretaceous strata in the Lhasa terrane, southern Tibet: Basin Research, v. 19, p. 361–378, doi:10.1111/j.1365-2117.2007.00330.x.

Li, G., Liu, X., Pullen, A., Wei, J., Liu, X., Huang, F., and Zhou, X., 2010, Detrital-zircon geochronology and in-situ hafnium (Hf) isotopic analyses of the Late Triassic Tethys Himalaya Sequence: Implications for provenance and tectonic setting: Earth and Planetary Science Letters, v. 297, no. 3–4, p. 461–470.

Li, X.H., Zeng, Q.G., and Wang, C.S., 2003a, Palaeocurrent data: Evidence for the source of the Langjiexue Group in southern Tibet: Geological Review, v. 49, no. 2, p. 132–137.

Li, X.H., Zeng, Q.G., and Wang, C.S., 2003b, Sedimentary characteristics of the Upper Triassic Langjiexue Group in southern Qingjie, Tibet: Geoscience, v. 17, no. 1, p. 52–58.

Li, X.H., Zeng, Q.G., and Wang, C.S., 2004, Provenance analysis of the Upper Triassic Langjiexue Group in southern Tibet, China: Acta Sediment Sinica, v. 22, no. 4, p. 553–559.

Liang, Y.-H., Chung, S.-L., Liu, D., Xu, Y., Wu, F.-Y., Yang, J.-H., Wang, Y., and Lo, C.-H., 2008, Detrital zircon evidence from Burma for reorganization of the eastern Himalayan river system: American Journal of Science, v. 308, p. 618–638.

Long, S., and McQuarrie, N., 2010, Placing limits on channel flow: Insights from the Bhutan Himalaya: Earth and Planetary Science Letters, v. 290, p. 375–390, doi:10.1016/j.epsl.2009.12.033.

Long, S., McQuarrie, N., Tobgay, T., Rose, C., Gehrels, G., and Grujic, D., 2011a, Tectonostratigraphy of the Lesser Himalaya of Bhutan: Implications for the along-strike stratigraphic continuity of the northern Indian margin: Geological Society of America Bulletin, v. 123, p. 1406–1426, doi:10.1130/B30202.1.

Long, S., McQuarrie, N., Tobgay, T., and Grujic, D., 2011b, Geometry and crustal shortening of the Himalayan fold-thrust belt, eastern and central Bhutan: Geological Society of America Bulletin, v. 123, p. 1427–1447, doi:10.1130/B30203.1.

Long, S., McQuarrie, N., Tobgay, T., and Hawthorne, J., 2011c, Quantifying internal strain and deformation temperature in the eastern Himalaya, Bhutan: Implications for the evolution of strain in thrust sheets: Journal of Structural Geology, v. 33, p. 579–608, doi:10.1016/j.jsg.2010.12.011.

Martin, A.J., DeCelles, P.G., Gehrels, G.E., Patchett, P.J., and Isachsen, C., 2005, Isotopic and structural constraints on the location of the Main Central thrust in the Annapurna Range, central Nepal Himalaya: Geological Society of America Bulletin, v. 117, p. 926–944, doi:10.1130/B25646.1.

McKenzie, R.N., Hughes, N.C., Myrow, P.M., Choi, D.K., and Park, T.Y., 2011, Trilobites and zircons link north China with the eastern Himalaya during the Cambrian: Geology, v. 39, p. 591–594, doi:10.1130/G31838.1.

McQuarrie, N., Robinson, D., Long, S., Tobagay, T., Grujic, D., Gehrels, G., and Ducea, M., 2008, Preliminary stratigraphic and structural architecture of Bhutan: Implications for along-strike architecture of the Himalayan system: Earth and Planetary Science Letters, v. 272, p. 105–117, doi:10.1016/j.epsl.2008.04.030.

Metcalfe, R.P., 1993, Pressure, temperature and time constraints on metamorphism across the Main Central Thrust zone and High Himalayan slab in the Garhwal Himalaya, *in* Treloar, P.J., and Searle, M.P., eds., Himalayan Tectonics: Geological Society London Special Publication 74, p. 485–509.

Meyer, M.C., Wiesmayr, G., Brauner, M., Hausler, H., and Wangda, D., 2006, Active tectonics in eastern Lunana (NW Bhutan): Implications for the seismic and glacial hazard potential of the Bhutan Himalaya: Tectonics, v. 25, TC3001, doi:10.1029/2005TC001858.

Mitra, G., Bhattacharyya, K., and Mukul, M., 2010, The Lesser Himalayan duplex in Sikkim: Implications for variations in Himalayan shortening: Journal of the Geological Society of India, v. 75, p. 289–301, doi:10.1007/s12594-010-0016-x.

Mitra, S.K., and Mitra, S.C., 2001, Tectonic setting of the Precambrian of north-eastern India (Meghalaya Plateau) and age of the Shillong Group of rocks: Geological Survey of India Special Publication 64, p. 653–658.

Mukherjee, S., and Koyi, H.A., 2010, Higher Himalayan Shear Zone, Zanskar Indian Himalaya: Microstructural studies and extrusion mechanism by a combination of simple shear and channel flow: International Journal of Earth Sciences (Geologische Rundschau), v. 99, p. 1083–1110.

Myrow, P.M., Hughes, N.C., Paulsen, T.S., Willlams, I.S., Parcha, S.K., Thompson, K.R., Bowring, S.A., Peng, S.C., and Ahluwalia, A.D., 2003, Integrated tectonostratigraphic analysis of the Himalaya and implications for its tectonic reconstruction: Earth and Planetary Science Letters, v. 212, p. 433–441, doi:10.1016/S0012-821X(03)00280-2.

Myrow, P.M., Thompson, K.R., Hughes, N.C., Paulsen, T.S., Sell, B.K., and Parcha, S.K., 2006, Cambrian stratigraphy and depositional history of the northern Indian Himalaya, Spiti Valley, north-central India: Geological Society of America Bulletin, v. 118, p. 491–510, doi:10.1130/B25828.1.

Myrow, P.M., Hughes, N.C., Searle, M.P., Fanning, C.M., Peng, S.C., and Parcha, S.K., 2009, Stratigraphic correlation of Cambrian–Ordovician deposits along the Himalaya: Implications for the age and nature of rocks in the Mount Everest region: Geological Society of America Bulletin, v. 121, p. 323–332, doi:10.1130/B26384.1.

Myrow, P.M., Hughes, N.C., Goodge, J.W., Fanning, C.M., Williams, I.S., Peng, S.C., Bhargava, O.N., Parcha, S.K., and Pogue, K.R., 2010, Extraordinary transport and mixing of sediment across Himalayan central Gondwana during the Cambrian–Ordovician: Geological Society of America Bulletin, v. 122, p. 1660–1670, doi:10.1130/B30123.1.

Nàbelek, J., Hetényi, G., Vergne, J., Sapkota, S., Kafle, B., Jiang, M., Su, H., Chen, J., Huang, B.-S., and the Hi-CLIMB Team, 2009, Underplating in the Himalaya-Tibet collision zone revealed by the Hi-CLIMB experiment: Science, v. 325, no. 5946, p. 1371–1374, doi:10.1126/science.1167719.

Nelson, K.D., et al., 1996, Partially molten middle crust beneath southern Tibet: Synthesis of Project INDEPTH results: Science, v. 274, p. 1684–1688, doi:10.1126/science.274.5293.1684.

Pan, G.T., Ding, J., Yao, D., and Wang, L., 2004, Geological Map of Qinghai-Xiang (Tibet) Plateau and Adjacent Areas: Chengdu, China, Chengdu Institute of Geology and Mineral Resources, China Geological Survey, Chengdu Cartographic Publishing House, scale 1:1,500,000.

Press, W.H., Teukolsky, S.A., Vetterling, W.T., and Flannery, B.P., 2007, Numerical Recipes: The Art of Scientific Computing (Third Edition): New York, Cambridge University Press, 1235 p. + xxi.

Price, R.A., 1986, The southeastern Canadian Cordillera: Thrust faulting, tectonic wedging, and delamination of the lithosphere: Journal of Structural Geology, v. 8, p. 239–254, doi:10.1016/0191-8141(86)90046-5.

Rajendran, C.P., Rajendran, K., Duarah, B.P., Baruah, S., and Earnest, A., 2004, Interpreting the style of faulting and paleoseismicity associated with the 1897 Shillong, northeast India, earthquake: Implications for regional tectonics: Tectonics, v. 23, doi:10.1029/2003TC001605.

Ratschbacher, L., Frisch, W., Liu, G., and Chen, C., 1994, Distributed deformation in southern and western Tibet during and after the India-Asia collision: Journal of Geophysical Research, v. 99, p. 19,917–19,945, doi:10.1029/94JB00932.

Ray, S.K., Bandyopadhyay, B.K., and Razdan, R.K., 1989, Tectonics of a part of the Shumar allochthon in eastern Bhutan: Tectonophysics, v. 169, p. 51–58, doi:10.1016/0040-1951(89)90182-0.

Richards, A., Argles, T., Harris, N., Parrish, R.R., Ahmad, T., Darbyshire, F., and Draganits, E., 2005, Himalayan architecture constrained by isotopic tracers from clastic sediments: Earth and Planetary Science Letters, v. 236, p. 773–796, doi:10.1016/j.epsl.2005.05.034.

Richards, A., Parrish, R., Harris, N., Argles, T., and Zhang, L., 2006, Correlation of lithotectonic units across the eastern Himalaya, Bhutan: Geology, v. 34, p. 341–344, doi:10.1130/G22169.1.

Robinson, D.M., DeCelles, P.G., Garzione, C.N., Pearson, O.N., Harrison, T.M., and Catlos, E.J., 2003, Kinematic model for the Main Central thrust in Nepal: Geology, v. 31, p. 359–362, doi:10.1130/0091-7613(2003)031<0359:KMFTMC>2.0.CO;2.

Robinson, D.M., DeCelles, P.G., and Copeland, P., 2006, Tectonic evolution of the Himalayan thrust belt in western Nepal: Implications for channel flow models: Geological Society of America Bulletin, v. 118, p. 865–885, doi:10.1130/B25911.1.

Schmitt, A.K., Grove, M., Harrison, T.M., Lovera, O.M., Hulen, J., and Walters, M., 2003, The Geysers–Cobb Mountain magma system, California (Part 1): U-Pb zircon ages of volcanic rocks, conditions of zircon crystallization and magma residence times: Geochimica et Cosmochimica Acta, v. 67, no. 18, p. 3423–3442, doi:10.1016/S0016-7037(03)00140-6.

Schneider, C., and Masch, L., 1993, The metamorphism of the Tibetan series from the Manang area, Marsyandi valley, central Nepal, *in* Treloar, P.J., and Searle, M.P., eds., Himalayan Tectonics: Geological Society of London Special Publication 74, p. 357–374.

Searle, M.P., 1986, Structural evolution and sequence of thrusting in the high Himalayan, Tibetan-Tethys and Indus suture zones of Zanskar and Ladakh, western Himalaya: Journal of Structural Geology, v. 8, p. 923–925, 927–936, doi:10.1016/0191-8141(86)90037-4.

Searle, M.P., 2001, A new geological map of Mount Everest: Journal of Asian Earth Sciences, v. 19, p. 59.

Searle, M.P., Law, R.D., Godin, L., Larson, K.P., Streule, M.J., Cottle, J.M., and Jessup, M.J., 2008, Defining the Himalayan Main Central thrust in Nepal: Journal of the Geological Society of London, v. 165, p. 523–534, doi:10.1144/0016-76492007-081.

Stacey, J.S., and Kramers, J.D., 1975, Approximation of terrestrial lead isotope evolution by a two-stage model: Earth and Planetary Science Letters, v. 26, p. 207–221, doi:10.1016/0012-821X(75)90088-6.

Stüwe, K., and Foster, D., 2001, Ar-40/Ar-39, pressure, temperature and fission-track constraints on the age and nature of metamorphism around the Main Central thrust in the eastern Bhutan Himalaya: Journal of Asian Earth Sciences, v. 19, p. 85–95, doi: 10.1016/ S1367-9120(00)00018–3.

Tangri, S.K., Bhargava, O.N., and Pande, A.C., 2003, Late Precambrian–Early Cambrian trace fossils from Tethyan Himalaya, Bhutan, and their bearing on the Precambrian-Cambrian boundary: Journal of the Geological Society of India, v. 62, p. 708–716.

Taylor, M., Yin, A., Ryerson, F., Kapp, P., and Ding, L., 2003, Conjugate strike slip fault accommodates coeval north-south shortening and east-west extension along the Bangong-Nujiang suture zone in central Tibet: Tectonics, v. 22, doi:10.1029/2002TC001361.

Tewari, V.C., 2001, Discovery and sedimentology of microstromatolites from Menga Limestone (Neoproterozoic/Vendian), Upper Subansiri District, Arunachal Pradesh, NE Himalaya, India: Indian Current Science Association, v. 80, p. 1440–1444.

Tobgay, T., Long, S., McQuarrie, N., Tobgay, T., Ducea, M.N., and Gehrels, G., 2010, Using isotopic and chronologic data to fingerprint strata: Challenges and benefits of variable sources to tectonic interpretations, the Paro Formation, Bhutan Himalaya: Tectonics, v. 29, TC6023, doi:10.1029/2009TC002637.

Upreti, B.N., 1999, An overview of the stratigraphy and tectonics of the Nepal Himalaya: Journal of Asian Earth Sciences, v. 17, p. 577–606, doi:10.1016/S1367-9120(99)00047-4.

Valdiya, K.S., 1980, Geology of Kumaun Lesser Himalaya: Dehra Dun, India, Wadia Institute of Himalayan Geology, 291 p.

van Breemen, O., Bowes, D.R., Bhattacharyya, and Chowdhary, P.K., 1989, Late Proterozoic–early Paleozoic Rb-Sr whole and mineral ages for granite and pegmatite, Goalpara, Assam, India: Journal of the Geological Society of India, v. 33, p. 89–92.

Vannay, J.C., and Grasemann, B., 1998, Inverted metamorphism in the High Himalaya of Himachal Pradesh (NW India): Phase equilibria versus thermobarometry: Schweizerische Mineralogische und Petrographische Mitteilungen, v. 78, p. 107–132.

Vannay, J.C., Grasemann, B., Rahn, M., Frank, W., Carter, A., Baudraz, V., and Cosca, M., 2004, Miocene to Holocene exhumation of metamorphic crustal wedges in the NW Himalaya: Evidence for tectonic extrusion coupled to fluvial erosion: Tectonics, v. 23, TC1014, doi:10.1029/2002TC001429.

Wagner, T., Lee, J., Hacker, B.R., and Seward, G., 2010, Kinematics and vorticity in Kangmar Dome, southern Tibet: Testing midcrustal channel-flow models for the Himalaya: Tectonics, v. 29, TC6011, doi: 10.1029/2010TC002746.

Warren, C.J., Grujic, D.; Kellett, D.A., and Cottle, J.C., 2011, Probing the depths of the India-Asia collision: U-Th-Pb monazite chronology of granulites from NW Bhutan: Tectonics, v. 30, TC2004, doi:10.1029/2010TC002738.

Webb, A.A.G., Yin, A., Harrison, T.M., Célérier, J., and Burgess, W.P., 2007, The leading edge of the Greater Himalayan Crystallines revealed in the NW Indian Himalaya: Implications for the evolution of the Himalayan orogen: Geology, v. 35, p. 955–958, doi:10.1130/G23931A.1.

Webb, A.A.G., Yin, A., Harrison, T.M., Célérier, J., Gehrels, G.E., Manning, C.E., and Grove, M., 2011a, Cenozoic tectonic history of the Himachal Himalaya (northwestern India) and its constraints on the formation mechanism of the Himalayan orogen: Geosphere, v. 7, p. 1013–1061, doi:10.1130/GES00627.1.

Webb, A.A.G., Schmitt, A.K., He, D., and Weigand, E.L., 2011b, Structural and geochronological evidence for the leading edge of the Greater Himalayan Crystalline complex in the central Nepal Himalaya: Earth and Planetary Science Letters, v. 304, p. 483–495, doi:10.1016/j.epsl.2011.02.024.

Wilson, J.T., 1966, Did the Atlantic close and then re-open?: Nature, v. 211, p. 676–681, doi:10.1038/211676a0.

Yin, A., 1989, Origin of regional rooted low-angle normal faults: A mechanical model and its implications: Tectonics, v. 8, p. 469–482, doi:10.1029/TC008i003p00469.

Yin, A., 2006, Cenozoic tectonic evolution of the Himalayan orogen as constrained by along-strike variation of structural geometry, exhumation history, and foreland sedimentation: Earth-Science Reviews, v. 76, p. 1–131, doi:10.1016/j.earscirev.2005.05.004.

Yin, A., and Harrison, T.M., 2000, Geologic evolution of the Himalayan-Tibetan orogen: Annual Review of Earth and Planetary Sciences, v. 28, p. 211–280, doi:10.1146/annurev.earth.28.1.211.

Yin, A., Harrison, T.M., Ryerson, F.J., Chen, W., Kidd, W.S.F., and Copeland, P., 1994, Tertiary structural evolution of the Gangdese thrust system, southeastern Tibet: Journal of Geophysical Research, v. 99, p. 18,175–18,201, doi:10.1029/94JB00504.

Yin, A., Harrison, T.M., Murphy, M.A., Grove, M., Nie, S., Ryerson, F.J., Feng, W.X., and Le, C.Z., 1999, Tertiary deformation history of southeastern and southwestern Tibet during the Indo-Asian collision: Geological Society of America Bulletin, v. 111, p. 1644–1664, doi:10.1130/0016-7606(1999)111<1644:TDHOSA>2.3.CO;2.

Yin, A., Dubey, C.S., Kelty, T.K., Gehrels, G.E., Chou, C.Y., Grove, M., and Lovera, O., 2006, Structural evolution of the Arunachal Himalaya and implications for asymmetric development of the Himalayan orogen: Current Science, v. 90, p. 195–206.

Yin, A., Dubey, C.S., Webb, A.A.G., Kelty, T.K., Grove, M., Gehrels, G.E., and Burgess, W.P., 2010a, Geological correlation of the Himalayan orogen and Indian craton: Part 1. Structural geology, U-Pb zircon geochronology, and tectonic evolution of the Shillong Plateau and its neighboring regions in NE India: Geological Society of America Bulletin, v. 122, p. 336–359, doi:10.1130/B26460.1.

Yin, A., Dubey, C.S., Kelty, T.K., Webb, A.A.G., Harrison, T.M., Chou, C.Y., and Célérier, J., 2010b, Geological correlation of the Himalayan orogen and Indian craton: Part 2. Structural geology, geochronology, and tectonic evolution of the eastern Himalaya: Geological Society of America Bulletin, v. 122, p. 360–395, doi:10.1130/B26461.1.

Zeng, L., Liu, J., Gao, L., Chen, F., and Xie, K., 2009, Early Mesozoic high-pressure metamorphism within the Lhasa block, Tibet, and implications for regional tectonics: Earth Science Frontiers, v. 16, p. 140–151, doi:10.1016/S1872-5791(08)60079-2.

Zhang, J., Santosh, M., Wang, X., Guo, L., Yang, X., and Zhang, B., 2012, Tectonics of the northern Himalaya since the India–Asia collision: Gondwana Research, v. 21, p. 939–960, doi:10.1016/j.gr.2011.11.004.

Zhang, R., Murphy, M., Lapen, T.J., Sanchez, V., and Heizler, M., 2011, Late Eocene crustal thickening followed by early-late Oligocene extension along the India-Asia suture zone: Evidence for cyclicity in the Himalayan orogen: Geosphere, v. 7, p. 1249–1268, doi:10.1130/GES00643.1.

Zhu, D., Pan, G., Mo, X., Wang, L., Liao, Z., Jiang, X., and Geng, Q., 2005, SHRIMP U-Pb zircon dating for the dacite of the Sangxiu Formation in the central segment of Tethyan Himalaya and its implications: Chinese Science Bulletin, v. 50, no. 6, p. 563–568.

Zhu, D., Pan, G., Mo, X., Liao, Z., Jiang, X., Wang, L., and Zhao, Z., 2007, Petrogenesis of volcanic rocks in the Sangxiu Formation, central segment of Tethyan Himalaya: A probable example of plume–lithosphere interaction: Journal of Asian Earth Sciences, v. 29, p. 320–335, doi:1016/j.jseaes.2005.12.004.

Zhu, D., Mo, X., Pan, G., Zhao, Z., Dong, G., Shi, Y., Liao, Z., Wang, L., and Zhou, C., 2008, Petrogenesis of the earliest Early Cretaceous mafic rocks from the Cona area of the eastern Tethyan Himalaya in south Tibet: Interaction between the incubating Kerguelen plume and the eastern Greater India lithosphere? Lithos, v. 100, p. 147–173, doi:10.1016/j.lithos.2007.06.024.

Zhu, D., Zhao, Z., Niu, Y., Mo, X., Chung, X., Hou, Z., Wang, L., and Wu, F., 2011, The Lhasa terrane: Record of a microcontinent and its histories of drift and growth: Earth and Planetary Science Letters, v. 301, p. 241–255, doi:10.1016/j.epsl.2010.11.005.

Science Editor: Christian Koeberl
Associate Editor: Stefano Mazzoli

Manuscript Received 12 October 2011
Revised Manuscript Received 12 July 2012
Manuscript Accepted 28 July 2012

Printed in the USA